5-2023

Graphene-Conductive Ink Coated Laser Engraved Kapton Electrochemical Biosensor for the Detection of Dopamine and Immune Sensing

Dipannita Ghosh
The University of Texas Rio Grande Valley

GRAPHENE-CONDUCTIVE INK COATED LASER ENGRAVED KAPTON ELECTROCHEMICAL BIOSENSOR FOR THE DETECTION OF DOPAMINE AND IMMUNE-SENSING

A Thesis

by

DIPANNITA GHOSH

Submitted in Partial Fulfillment of the

Requirements for the Degree of

MASTER OF SCIENCE IN ENGINEERING

Major Subject: Electrical Engineering

The University of Texas Rio Grande Valley

May 2023

GRAPHENE-CONDUCTIVE INK COATED LASER ENGRAVED KAPTON ELECTROCHEMICAL BIOSENSOR FOR THE DETECTION OF DOPAMINE AND IMMUNE-SENSING

A Thesis
by
DIPANNITA GHOSH

COMMITTEE MEMBERS

Dr. Nazmul Islam
Chair of Committee

Dr. Ali Ashraf
Co-Chair of Committee

Dr. Paul Choi
Committee Member

May 2023

ABSTRACT

Ghosh, Dipannita, Graphene-Conductive Ink Coated Laser Engraved Kapton Electrochemical Biosensor for the Detection of Dopamine and Immune-Sensing. Master of Science in Engineering (MS), May, 2023, 58 pp., 8 tables, 42 figures, references, 67 titles.

Novel and flexible disposable laser-engraved Kapton (LEK) electrodes modified with graphene conductive inks have been developed for dopamine and Interleukin-6 (IL-6) detection. The LEK sensors exhibit high reproducibility (RSD=0.76%, N=5) and stability (RSD=4.39%, N=15) after multiple bendings, and thus make the sensors ideal for wearable and stretchable bioelectronics applications. We have developed graphene conductive ink- PEDOT:PSS (G-PEDOT:PSS) and polyaniline (G-PANI) based electrode coatings for working electrode modification to improve the sensitivity (41.41 times higher for screen printed electrode with G-PEDPT:PSS ink modification), and limit of detection (LOD) . We have further compared the performance of the fabricated electrodes with commercially available screen-printed electrodes (SPE), screen-printed electrodes modified with G-PEDOT:PSS (SPE/G-PEDOT:PSS) and G-PANI (SPE/G-PANI). SPE/G-PANI has a lower LOD of 0.632 μM, compared to SPE/G-PEDOT:PSS (0.867 μM) and SPE/G-PANI (1.974 μM). The lowest LOD of the LEK/G-PANI sensor (0.4084 μM, S/N=3) suggests that it can be a great alternative to measure dopamine levels in a physiological medium. Additionally, LEK/G-PANI electrode has excellent LOD (2.6234 pg/mL) to detect IL-6.

DEDICATION

I would like to express my sincere gratitude to my mother and Amit for their unwavering love, support, and encouragement throughout my academic journey. Their support has been an immense source of strength and motivation for me.

ACKNOWLEDGMENTS

First of all, I would like to thank the Almighty for keeping me healthy and safe.

I will always be indebted to my supervisor Dr. Nazmul Islam, and co-supervisor Dr. Ali Ashraf not only for his support as a mentor and a guide for my research but also for being humble and generous human beings for their continuous support and motivation.

I would like to thank my committee member Dr. Paul Choi for being part of my thesis committee.

Finally, Kudos to Amit and my parents for being a constant support.

TABLE OF CONTENTS

Page

LIST OF TABLES

Page

LIST OF FIGURES

CHAPTER I

INTRODUCTION

1.1 Background of Electrochemistry

The link between electrical values, such as current, potential, or charge, and chemical parameters is the focus of electroanalytical techniques, which measure electrical quantities[67]. Applications for using electrical measurements for analytical purposes are numerous and include biological analysis, industrial quality control, and environmental monitoring. Since the middle of the 1980s, there have been advancements in the design of ultramicroelectrodes, the creation of molecular monolayers and tailored interfaces, the coupling of biological elements and electrochemical transducers, the creation of ionophores and receptors with molecular-sized cavities, the development of ultratrace voltammetric techniques or high-resolution scanning probe microscopies, the microfabrication of molecular devices, and the development of effective flow detectors[50]. Potentiometric and potentiostatic measurements are electroanalytical measurements. Both kinds need an electrochemical cell, which consists of a contacting sample (electrolyte solution) and at least two electrodes (conductors). Hence, an ionic conductor and an electronic conductor meet at the electrode surface. The indicator (or functioning) electrode is the one of the two electrodes that reacts to the target analyte(s)[17]. The second electrode, often known as the reference electrode, has a constant potential and is therefore unaffected by the characteristics of the solution. Galvanic electrochemical cells are those that generate electricity whereas electrolytic electrochemical cells are those that either consume electricity from an external source or both.

1.2 Application of Electrochemistry

Electrochemical processes have a wide range of applications, and their use is expected to grow due to their ability to replace polluting chemical processes with environmentally friendly ones. Many fields have already been benefiting from electrochemistry for some time, and the major categories of its applications are discussed below[10].

Metallurgy: With the exception of iron and steel, most technologically important metals are obtained or refined using electrochemical processes. For example, aluminum, titanium, alkaline earth, and alkali metals are obtained by electrodeposition from molten salts, while copper is refined by electrolysis in aqueous copper sulfate solutions[14].

Electroplating: Electroplating is a major method for enhancing the corrosion resistance of objects and for decorating them. The majority of metal-working industries, particularly the automobile industry, have large electroplating plants[61].

Chemical industry: The electrolysis of brine to obtain chlorine and caustic soda is an electrochemical process that has become one of the largest volume productions in the chemical industry. Modern processes cover a wide field, from the production of various inorganic compounds to the production of synthetic fibers such as nylon. Significant advancements in organic electrochemistry are expected due to intensive research, especially with the possibility of substantially reduced electricity costs from controlled fusion development in the future[34].

Battery:Batteries are the primary means of electrochemical energy storage. Electrochemical cells, which consist of two electrodes per unit, are utilized in this devices[47]. When electricity is supplied to the cell's plates, it converts the substances on the plates into new substances with higher energy levels. To make the electricity available again, the battery's terminals are connected to the load, and the substances on the plates are transformed back into their original state, releasing electricity through electrochemical reactions[36]. Lead-acid batteries are extensively used for starting internal combustion engines, and their production has increased steadily over time. Other electrochemical systems, such as nickel-iron (Edison cell) and nickel-cadmium batteries with alkaline electrolytes, are employed in applications requiring longer lifetimes than lead-acid batteries.

The silver-zinc battery is used to start airplane engines because of its high power-to-weight ratio. Researchers are investigating various new systems to meet other energy storage requirements[38]. One of the greatest challenges for electrochemists and electrochemical engineers is to create a battery that has enough power and energy density to run an automobile in a similar manner to gasoline (petrol)[63]. Even if the best hypothetical predictions for reducing pollutants from automobile exhaust are met, the cleanup will not be enough due to the anticipated growth of the automobile population and increased pollutant production rates[66].

Biology: The notion that numerous biological processes, ranging from blood clotting to the transmission of nerve impulses, are electrochemical in nature is becoming more widespread in the field of biology[8]. The conversion of food's chemical energy to mechanical energy in biological systems occurs with such high efficiency that it is challenging to explain without considering electrochemical mechanisms[1]. Extensive research is currently underway in bioelectrochemistry, exploring various avenues of inquiry[13].

1.3 Significance of Dopamine, IL-6 & Estrogen Detection

Dopamine is an important neurotransmitter that plays a crucial role in the regulation of various physiological and behavioural processes in the human body[20]. It is involved in the regulation of mood, movement, motivation, reward, attention, and learning, among others. Thus, the detection of dopamine is of great importance in many areas of research and clinical practice.For example, in the field of neurology and psychiatry, the measurement of dopamine levels in the brain is important for the diagnosis and treatment of various neurological and psychiatric disorders, such as Parkinson's disease, schizophrenia, depression, and addiction[62]. In Parkinson's disease, the degeneration of dopaminergic neurons in the brain leads to a decrease in dopamine levels, which results in motor symptoms such as tremors and rigidity[6]. Thus, the detection of dopamine levels in the brain can help in the early diagnosis and monitoring of the disease.

Interleukin-6 (IL-6) is a cytokine that plays a critical role in the immune system and inflammation. It is produced by various cells, including immune cells, and has a wide range of functions in the body[56]. The detection of IL-6 is important in many areas of research and

clinical practice.One important application of IL-6 detection is in the diagnosis and monitoring of inflammatory diseases such as rheumatoid arthritis, inflammatory bowel disease, and sepsis[2]. In these conditions, IL-6 levels are elevated, and the detection of IL-6 can be used as a biomarker for disease diagnosis and progression[16]. Additionally, IL-6 has been implicated in the pathogenesis of several other diseases, including cancer and cardiovascular disease. The detection of IL-6 in these diseases can aid in disease diagnosis and prognosis, as well as in the development of targeted therapies[52].

Estrogen is a hormone that plays a critical role in the development and functioning of the female reproductive system, as well as in the regulation of various physiological processes in both males and females[41]. The detection of estrogen is important in many areas of research and clinical practice. One important application of estrogen detection is in the diagnosis and monitoring of reproductive health in women[31]. Estrogen levels fluctuate during the menstrual cycle, and the measurement of estrogen levels can be used to track ovulation and diagnose reproductive disorders such as polycystic ovary syndrome and menopause[46]. In addition, the detection of estrogen levels is important in monitoring the effectiveness of hormone replacement therapy in menopausal women[27]. Moreover, estrogen has been implicated in the pathogenesis of various diseases, including breast cancer, prostate cancer, and osteoporosis. The detection of estrogen levels can aid in the diagnosis, prognosis, and treatment of these diseases [28].

1.4 Electrochemical Biosensors

An electrochemical biosensor is a type of biosensor that utilizes electrochemical techniques to detect and quantify biological molecules or analytes[65]. It consists of a biological recognition element (such as an enzyme, antibody, or nucleic acid) that is immobilized onto an electrode surface, and a transducer that converts the chemical signal generated by the biological reaction into an electrical signal[19]. When the target analyte binds to the recognition element, a reaction occurs that produces an electrical signal. This signal can be measured and used to quantify the amount of the analyte in the sample. The advantages of electrochemical biosensors include their high sensitivity, specificity, and speed of analysis.

CHAPTER II

LITERATURE REVIEW

2.1 Theory of Electrochemical Process

2.1.1 Faradic Process

The objective of controlled-potential electroanalytical experiments is to obtain a current response that is related to the concentration of the target analyte[22]. Such an objective is accomplished by monitoring the transfer of electron(s) during the redox process of the analyte:

$$0 + ne^{-} = R \tag{2.1}$$

where O and R are the oxidized and reduced forms, respectively, of the redox couple. Such a reaction will occur in a potential region that makes the electron transfer thermodynamically or kinetically favorable. For systems controlled by the laws of thermodynamics, the potential of the electrode can be used to establish the concentration of the electroactive species at the surface [CO(0,t) and CR(0,t)] according to the Nernst equation [59]. The electrode response follows a pathway that can be fairly intricate and comprises a number of phases. The slowest stage in the chain determines how quickly these reactions occur [**?**]. The only steps in simple reactions are the mass transport of the electroactive species to the electrode surface, the transfer of electrons across the interface, and the transport of the finished product back to the bulk solution. Other chemical and surface processes that either come before or after the actual electron transfer are part of more complicated reactions[9]. The either mass movement of the reactant or the rate of electron transfer may be a constraint on the reaction's overall pace and, consequently, the measured current. The rate-determining step will be a slower process [51]. The type of molecule being measured and

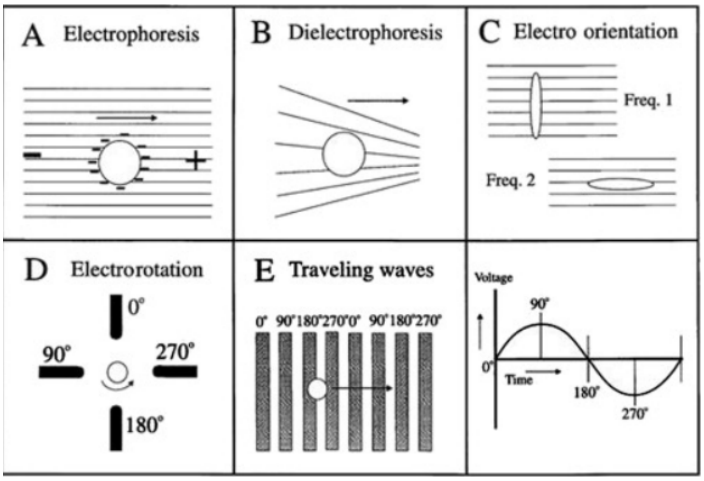

Figure 2.1: Main Electrokintetics Phenomena Outline[57]

different experimental variables (electrode material, medium, operating potential, mode of mass transport, time scale, etc.) usually indicate whether a given reaction is governed by mass transport or electron transfer [32]. The rate-determining step may thus be dependent on the potential range being studied for a particular system.

2.1.2 Mass Transport Controlled Reaction

Three different modes of mass transportation exist[23]:

• Diffusion is the naturally occurring transition between high and low concentration areas under the influence of a concentration gradient with the goal of decreasing concentration discrepancies[29].

• Convection is the physical movement that transports an electrode to the electrode; the main driving factor behind convection is external mechanical energy that is used to stir or flow the solution or to rotate or vibrate the electrode (i.e., forced convection). Density gradients can also cause convection in a natural environment[42].

• Migration is the movement of charged particles along an electrical field (i.e. when ions carry the charge through a solution based on the number of transference units they possess) [54].

These modes of mass transport are illustrated in Figure 2.1. The flux (J), a common measure of the rate of mass transport at a fixed point, is defined as the number of molecules penetrating a unit

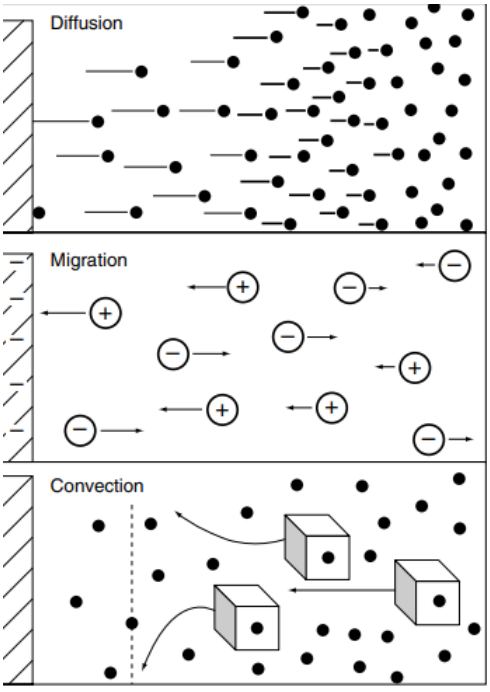

Figure 2.2: Three modes of mass transport[45]

area of an imaginary plane in a unit of time. The flux to the electrode is described mathematically by a differential equation, known as the Nernst–Planck equation, given here for one dimension[37].

In aqueous media, D usually ranges between 105 and 106 cm2/s. The current (i) is directly proportional to the flux and the surface area (A)

$$i = -nAFJ \tag{2.2}$$

Eq. (2.2) shows that the situation is rather complicated when all three mass transportation modalities are present at the same time. It is challenging to connect the current to the analyte concentration because of this issue. By reducing the electromigration by adding too much inert salt, the problem can be made much simpler. By increasing the conductivity of the solution, the addition of a high concentration of the supporting electrolyte (relative to the concentration of electroactive ions) aids in the reduction of the electrical field [64]. Using a quiescent solution will eliminate convection effects. Diffusion controls the mobility of the electroactive species in the absence of migration and convection effects. A diffusional flux is produced as a result of the reaction at the electrode's

surface, which also creates a concentration gradient nearby. So, many electroanalytical procedures can benefit from understanding the equations regulating diffusion processes[3].

2.1.3 Electrical Double Layer

At every material interface, there is an array of charged particles and/or oriented dipoles known as an electrical double layer[18]. To balance off the excess charge on the electrode in electrochemistry, such a layer reflects the ionic zones created in the solution (qe). Hence, a layer of negatively charged ions is drawn to a positively charged electrode (and vice versa). Because of the neutral interface, qe + qs =0. As a result, such a counter layer is made up of ions with the electrode's opposite sign. The electrical double layer has a complex structure made up of multiple unique sections, as shown in Figure 2.2.

Helmholtz proposed the oldest model for the double-layer structure at metal electrodes, depicted in Figure 2.3. It states that in the absence of specific adsorption, the surface of the electrode is coated with a layer of water molecules, and the ions can only access the second layer whose center is referred to as the outer Helmholtz plane[7]. According to Helmholtz's assumption, all of the excess charges of the solution reside in this plane. This model is qualitatively correct at high ionic concentrations where the solution's conductivity is high, and its excess charge should be located at the surface. In this model, the interface behaves like a parallel plate capacitor, and the effective plate separation is determined by the distance between the outer Helmholtz plane and the metal surface, which is approximately 0.4 nm. The intervening water layer functions as a dielectric because it consists of a monolayer of water only, and its dielectric constant (epsilon) is considerably lower than that of bulk water.

At high ionic concentrations, the Helmholtz model provides a reasonable description of the double-layer structure. However, it fails to explain the behavior at low concentrations, which was addressed by Gouy and Chapman's first statistical double-layer theory presented at the beginning of the last century. This theory has much in common with the Debye-Hückel theory developed several decades later[30].

The Gouy-Chapman theory[4] focuses on a planar metal electrode immersed in an ionic

solution and begins with the following assumptions: (1) the metal is a perfect conductor, and its excess charge is uniformly distributed on the surface; (2) the solvent is a dielectric continuum with a dielectric constant; and (3) the ions are point particles whose distribution is determined by the Poisson-Boltzmann equation[35]. For an electrolyte containing cations and anions with the same charge number z, explicit expressions for the differential capacity and electrostatic potential profile can be derived. The quantity commonly measured is the differential capacity per unit area:

$$C = \frac{\partial \Phi}{\partial t} \tag{2.3}$$

where σ is the charge per unit area of the electrode and ϕ the electrode potential.

Potentiometry is a technique that passively measures the potential of a solution between two electrodes, with minimal effect on the solution[11]. The two electrodes used are the reference electrode, which has a constant potential, and the indicator electrode, whose potential changes with the sample's composition. The difference in potential between the two electrodes provides information about the sample's composition. Potentiometric measurements are non-destructive and measure the solution's potential assuming the electrode is in equilibrium with the solution. Indicator electrodes made selectively sensitive to the ion of interest are commonly used in potentiometry, such as fluoride selective electrodes for measuring fluoride ions. The time taken for the electrode to reach equilibrium with the solution affects the measurement's sensitivity and accuracy. In aquatic environments, platinum is often used due to its high electron transfer kinetics, but electrodes made from several metals can be used to enhance electron transfer kinetics. The most commonly used potentiometric electrode is the glass-membrane electrode in a pH meter.

Coulometry is a technique that utilizes applied potential or current to completely convert an analyte from one oxidation state to another [39]. The total current passed during the process is measured directly or indirectly to determine the number of electrons transferred. This information can be used to determine the concentration of the analyte or, when the concentration is known, the number of electrons involved in the redox reaction. Coulometry encompasses various methods such

as bulk electrolysis, also referred to as potentiostatic coulometry or controlled potential coulometry, as well as several types of coulometric titrations[53].

Voltammetry involves applying a constant and/or varying potential at the surface of an electrode and measuring the resulting current using a three-electrode system[54]. By doing so, it is possible to determine the reduction potential of an analyte and its electrochemical reactivity. Unlike some other methods, voltammetry is considered non-destructive, as only a very small amount of the analyte is consumed at the two-dimensional surface of the working and auxiliary electrodes. However, it is often difficult to separate the analyte from the bulk electrolyte, and therefore the solution is usually disposed of after the experiment. Typical voltammetry experiments involve 1-10 mL solution with an analyte concentration between 1 and 10 mmol/L, although more advanced techniques can work with much smaller volumes and lower concentrations. Chemically modified electrodes can be used for the analysis of both organic and inorganic samples.

2.1.4 Cyclic Voltammetry

Cyclic voltammetry is a widely used electroanalytical technique for acquiring qualitative information about electrochemical reactivity. It uses a three-electrode cell system, with a novel working electrode being the primary focus. A platinum wire is commonly used as the counter electrode, while a saturated calomel electrode serves as the reference electrode for electrochemical studies. Cyclic voltammetry is particularly useful for studying interfacial processes and soluble reaction intermediates. This technique records the current response of a small stationary microelectrode as a function of a triangular potential waveform. Pulse voltammetric techniques are aimed at lowering the detection limit of voltammetric measurements[21]. Cyclic voltammetry is a valuable technique for investigating oxidation and reduction processes, as it allows for the generation of a species during the forward scan and subsequent observation of its fate during the reverse scan or subsequent cycles, all within a matter of seconds. One unique aspect of cyclic voltammetry is the use of a three-electrode system, consisting of a working electrode, a reference electrode, and a counter electrode. The working electrode acts as a medium with adjustable reductive or oxidative power via the applied potential, becoming a stronger oxidant or reductant as the potential is increased

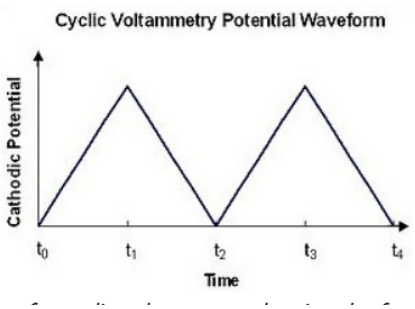

Figure 2.3: Cyclic Voltammetry Waveforms[25]

or decreased linearly over time. Typically, the working electrode is made of a chemically inert conductive material like platinum and serves as a donor or acceptor of electrons[44]. The general reaction, involves the addition of electrons to the oxidized electrode and its transformation to its most reduced form.

$$0 + ne^{-} = R \tag{2.4}$$

The potential difference between the working and reference electrodes is kept constant by the reference electrode, which is typically made of AgCl or calomel. The current flowing between the working and counter electrodes is measured, while the potential difference between the working and reference electrodes is measured as well. The counter electrode plays a critical role in ensuring accurate measurements since it prevents the current from passing through the reference electrode, which could alter its potential. A voltage sweep is generated using a signal generator, ranging from the initial voltage (Ei) to the final voltage (Ef), which is then applied to the working electrode via a potentiostat, an external power source. By slowly sweeping the voltage, information about the sample can be obtained from a graph of potential versus current. This technique, known as polarography, involves analyzing the limited current resulting from a redox process in the solution during the voltage sweep. This information can be used to quantitatively determine the concentration of electrochemically active species present in the solution[48]. There are two key differences between CV and polarography. The first is that the working electrode used in CV maintains a constant surface area, in contrast to classical polarography where the electrode surface

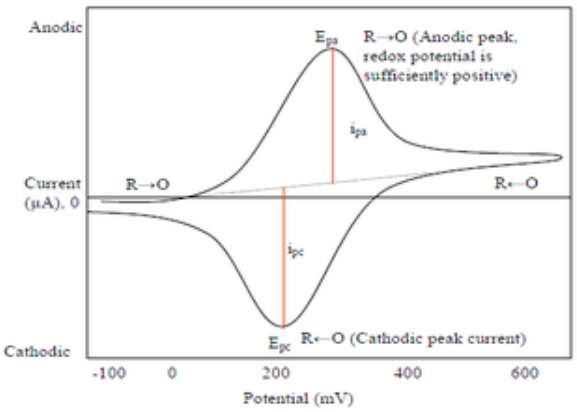

Figure 2.4: Cyclic Voltammogram[26]

changes over time. This electrode can be made of solid materials such as platinum or graphite with a small surface area, or it can be a stationary or hanging mercury drop that is periodically renewed. The second difference is that in CV, the potential of the working electrode is rapidly scanned over a wide potential range and then returned to its initial value using a linearly varying applied potential signal between the initial and final values. Typically, this technique is used to observe reduction currents during the forward scan and oxidation currents during the reverse scan. Figure 2.5 shows a typical cyclic voltammogram resulting from a potential versus time profile.

Effect of scan rate in Cyclic Voltammetry: Cyclic voltammetry offers the unique advantage of exploring the electrochemical behavior of species generated at the electrode by scanning the potential in both directions[55]. This sets it apart from other voltammetric techniques. For instance, the cyclic voltammogram in the illustration below depicts the same redox couple at faster (a) and slower (b) scan rates[40]. The faster scan rate displays two peaks, whereas the reverse scan peak vanishes at the slower scan rate. This is due to the adequate time allowed for the products of the reduction of R during the forward scan to partake in a non-electroactive chemical reaction, which explains the disappearance of the reverse scan peak[5].

2.1.5 Electrochemical Impedance Spectroscopy

Electrochemical Impedance Spectroscopy (EIS) is a transfer-function measurement technique that is widely used to analyze linear time-invariant systems. However, in the case of elec-

trochemical systems, it is crucial to maintain a stationary state throughout the measurement. To achieve this, EIS employs small-amplitude potential or current periodic perturbations at different frequencies[59]. By measuring the system's response (current or potential) to these perturbations, a transfer function can be calculated, which represents the electrochemical impedance of the system, in the case of an electrochemical cell. The impedance, Z, can be expressed as:

$$Z(\omega) = \frac{V(\omega)}{I(\omega)} \tag{2.5}$$

In this equation, ω is the angular frequency, which is related to the frequency f (in Hertz) by $\omega = 2\pi f$. ϕ is the phase angle between the input and output signals, and $j = \sqrt{-1}$ is the imaginary unit. The variables $\widetilde{V}$ and $\widetilde{I}$ are phasors, which are complex time-invariant numbers that account for the amplitude and phase of a sinusoidal function.

The electrochemical impedance, as defined by Eq. (2.7), is a frequency-dependent complex number, whose real part, Z_r, is a frequency-dependent resistance, and imaginary part, Z_j, is a frequency-dependent reactance[43]. Although the International Union of Pure and Applied Chemistry (IUPAC) conventions hold that the real part should be represented by Z' and the imaginary part denoted by Z'', the use of primes can be easily confused with the notation for spatial derivatives in the engineering literature. Therefore, the notation used in the present work is that the real part is denoted by subscript 'r' and the imaginary part is denoted by subscript 'j'.

EIS measurements should adhere to the Kramers-Kronig relations[58] (Box 1), which are derived based on the assumptions that the system being studied is linear, stable, and causal (Equation 2.8).

$$Z(\omega) = -\frac{2\pi}{\omega}\int_0^\infty \frac{Z(x) - Z(\omega)}{x^2 - \omega^2} dx \tag{2.6}$$

The perturbation amplitude necessary to achieve a linear response with an appropriate signal-to-noise ratio should be determined experimentally for each system being investigated. While a typical amplitude for potentiostatic modulation is usually around 10 mV, amplitudes as large as 1 V may be used for the impedance response of high-resistivity lubricating fluids. The Kramers-Kronig

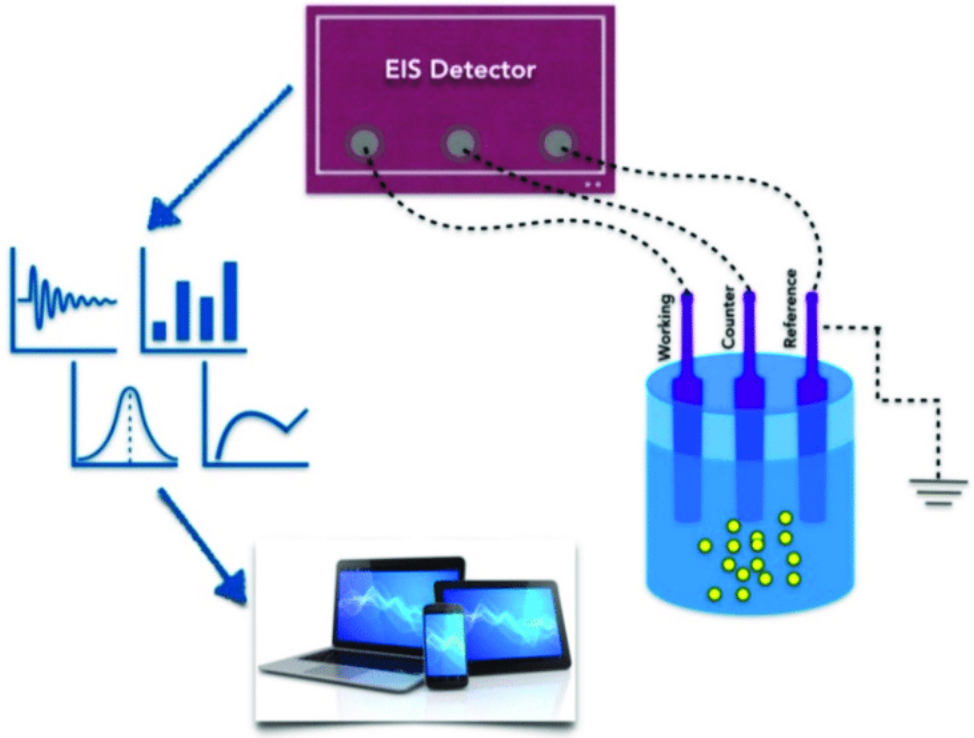

Figure 2.5: Schematic view of EIS[33]

relations[60] can be used as a tool to identify the uncorrupted portion of the measured frequency range, free from the instrument or non-stationary artifacts.

When Z real is plotted on the X-axis and Z imag on the Y-axis, a Nyquist plot is formed (Figure 2.7), right side). Each point on the Nyquist plot represents an impedance value at a specific frequency point where Z imag is negative. The right side of the plot corresponds to low-frequency conductance, while the left side corresponds to high-frequency resistance. In addition, impedance can be represented as a vector (arrow) of length |Z| on the Nyquist plot. The angle between this arrow and the X-axis is known as the "phase angle." Alternatively, the impedance results can be expressed using a Bode plot, which is more commonly used in the engineering community than the Nyquist plot. The Bode plot consists of two separate logarithmic plots: magnitude vs. frequency and phase vs. frequency.

The two forms of EIS are Faradaic and non-Faradaic. Faradaic impedance arises from redox reactions, while non-Faradaic impedance is DC-based and originates from double-layer capacitance. Faradaic current, which is related to electron transfer through electrode surfaces, is

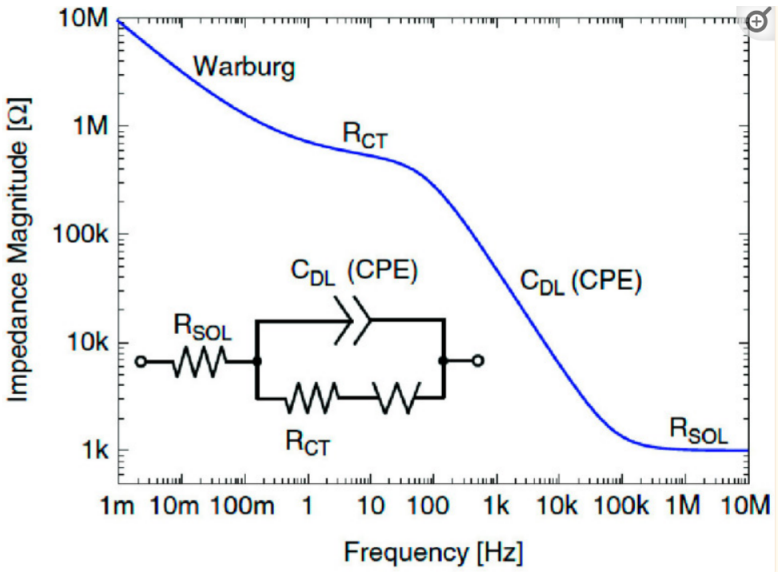

Figure 2.6: Bode Plot of an electrochemical interface comprising both non-Faradaic and Faradic phenomena[15]

used for quantitative analysis [14]. The capacitance of electrochemical systems can be determined using a Bode plot, which shows frequency versus phase angle. More information on Bode plots can be found in Scully and Silverman. In general, Bode plots are used to evaluate capacitive systems, while Nyquist plots are typically used for analyzing resistive processes. The overall impedance of a circuit with multiple components can be calculated by summing the impedances of each constituent, and Ohm's law can be applied in this case.

$$Z_{total} = Z_1 + Z_2 + Z_3 + \cdots + Z_x \tag{2.7}$$

An electric circuit, known as an equivalent circuit, is used to simulate and compute electrochemical processes related to electrolyte/interface and redox reactions. This circuit consists of various electrical components, such as resistors, capacitors, and inductors, which are designed and implemented to analyze individual components of the EIS system. In the Randles equivalent circuits, the resistance of the solution (Rs), double layer capacitance at the electrode surface (CdI), charge transfer resistance (Rct), and Warburg resistance (Zw) are simplified, as depicted in Figure 2.8. The Warburg resistance is a result of the diffusion process that occurs at the electrode-electrolyte interface. In

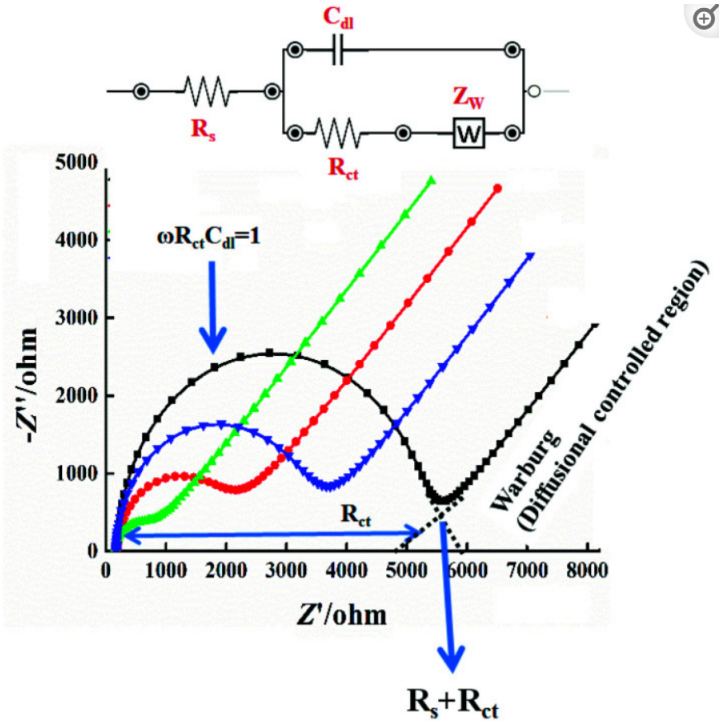

Figure 2.7: Stimulated EIS Spectra & Equivalent Circuit[12]

practice, a perfect capacitor is not usually available, hence an additional element called a constant phase element (CPE) is used to model this non-ideal capacitance behavior. This is because the investigated materials may have surface roughness, non-homogeneity, or surface porosity, among other factors[24]. The equivalent circuit components are determined and connected based on the shape of the Nyquist plot obtained from practical data. Therefore, obtaining the EIS curve is crucial before evaluating the surface characteristics by fitting the electrical circuit simulation. The electrode matrix, i.e., the composition of the working electrode, and the electrochemical responses occurring at the surface or in the bulk solution influence the shape of the Nyquist plot. As a result, different Nyquist plot curves, such as a single semicircle, two semicircles, or two half-semicircles, can be generated for specific electrochemical operations.

Three Electrode Electrochemical Sensor:The three-electrode system resolves several issues associated with the two-electrode setup. It comprises a working electrode, a counter electrode, and a reference electrode. The reference electrode acts as a standard for measuring and regulating the working electrode potential without passing any current. To achieve this, the reference electrode

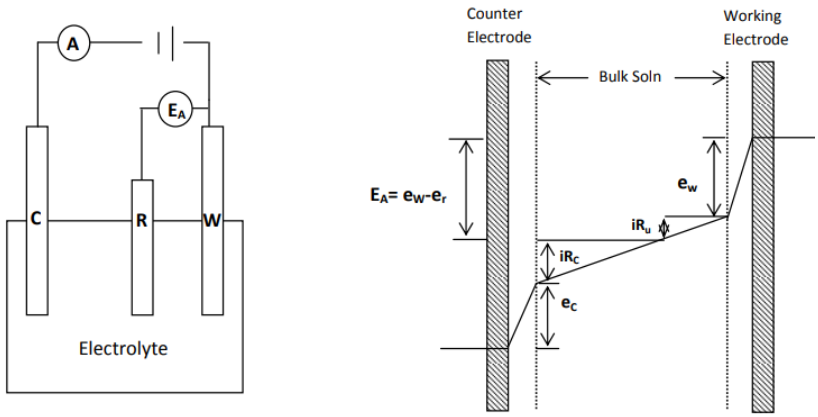

Figure 2.8: Schematic of three-electrode system

must maintain a consistent electrochemical potential at low current density. Moreover, since the reference electrode passes negligible current, the iR drop between it and the working electrode (iRU) is typically minimal. Consequently, the reference potential is much more stable, and compensation for iR drop across the solution is possible, leading to superior control over the working electrode potential. The most commonly used reference electrodes in the laboratory are the Saturated Calomel Electrode and the Ag/AgCl electrode. In the three-electrode configuration, the counter electrode only serves to conduct all the current required to balance the current observed at the working electrode. It often moves to extreme potential to achieve this task[49].

CHAPTER III

EXPERIMENTAL TOOLS & SOFTWARE

3.1 Autolab Potentiostat

The PGSTAT302N is the entry-level component of the Autolab modular instrument family, possessing a low current, low noise, and fast potentiostat/galvanostat. It is capable of measuring up to 800 mA, with a compliance voltage of 12 V, making it a suitable option for electrochemical measurements in small cells. The PGSTAT302N is a high-performance, cost-effective solution designed for a wide range of electrochemical applications, including corrosion measurements and energy storage device characterization. This budget-friendly instrument is an excellent option for electrochemical applications where performance is a priority. Additionally, the PGSTAT128N can be customized and expanded by incorporating one or more optional modules or accessories to enhance its capabilities. The device has a maximum current of 2A and can be boosted up to 20A, with a compliance voltage of 30V. It is controlled using NOVA software and additional features are listed in the table below:

The Autolab/PGSTAT302N comes with Autolab Dummy Cell, 50 cm BNC cable, Monitor Cables, and power cables.

Figure 3.1: Autolab/PGSTAT302N

Table 3.1: Autolab/PGSTAT302N Parameters

Features	Parameters
Electrode Connections	2,3,4
Potential Range	+-10V
Compliance Voltage	+-30V
Current Range	1 A to 10 nA
Maximum Current	+-2A
Potential Accuracy	+-0.2 percent
Current Resolution	0.0003 percent
Input Impedance	>10 Tohm
Potentiostat Bandwidth	1 MHz
Computer Interface	USB
Software	Nova 2.1
Electrode System	Three

3.1.1 Interfacing Nova 2.1 Software and Autolab

NOVA is a specialized software package that provides control of Autolab instruments via a USB interface. Developed by experienced electrochemists, NOVA incorporates over 20 years of user feedback and employs cutting-edge .NET software technology.

To run NOVA, your computer must have at least a 1 GHz 32-bit (x86) or 64-bit (x64) processor, a USB port, 2 GB of RAM, 20 GB of free hard disk space, a DirectX 9.0c compliant display adapter with 64 MB of RAM, and either Windows 7, Windows 8, or Windows 10.

NOVA is compatible with the following Autolab instruments: PGSTAT101, PGSTAT204, PGSTAT302, Multi Autolab/M204, Multi Autolab/M101, PGSTAT128N, AUT302N.MBA.S, and AUT128N.MBA.S.

The Steps to interface the Autolab Potentiostat with electrodes and Nova Software is described below:

Step 1: To set up the Autolab/PGSTAT302N, connect the sensor to the auto lab with the help of a port. Once the sensor is connected with Autolab, turn on the machine.

Step 2: In the laboratory, a dedicated PC is used to connect to the machine and run the Nova 2.1 software. The second step involves opening the software by clicking on the Nova 2.1 icon and selecting the "Open Library" option.

Step 3: Click on "Default Procedures" to open the cyclic voltammetry potentiostat.

Step 4 (Cyclic Voltammetry): After opening the default procedure, it will show different procedures. Among all of these, click on "Cyclic Voltammetry Potentiostatic"

Step 5 (Cyclic Voltammetry): Cyclic Voltammetry Potentiostatic window will open and click on CV staircase.

Step 6(Cyclic Voltammetry): After clicking CV Staircase, it will open another command box showing all the parameters of the cyclic voltammetry procedure(Figure 4.7). We can set all the parameters according to our preferences. Click more for additional settings.

The table is given below to provide the parameters of cyclic voltammetry

Table 3.2: Cyclic Voltammetry/Optimized Parameters

Parameters	**Value**
Upper Vortex Potential	0.35V
Lower Vortex Potential	-0.35V
Scan rate	0.08 V/sec
Step Potential	0 V

Step 7 (Cyclic Voltammetry): After clicking the run icon, the software will show the plots of the cyclic voltammetry procedure and after a certain time, the plots and data will be available. We can save the data as an excel file or ASCII. In our experiment, we saved the data in an excel file for further analysis.

Step 8 (Electrochemical Impedance Spectroscopy): When you open the library, it will display a number of commands. However, among those commands, FRA Impedance Potentiostatic must be selected and clicked to open in a new window. When the separate window for FRA Impedance Potentiostatic is open, click FRA Measurement to open another command box. After defining the parameters for the process, click on the run icon, and the process will be launched as shown in. In our experiments, we have used the Nyquist Plots.

Step 9 (Electrochemical Impedance Spectroscopy): Finally, the images and data collected must be exported to a specific folder or file. The plots are exported in.PNG or.JPEG format at a specific resolution, and Figure 4.18 depicts the data being extracted and exported in Excel format.

3.2 Vector Graphics Software Inventor

Autodesk Inventor is an advanced 3D CAD software that caters to the needs of mechanical designers, engineers, and manufacturing professionals. Its robust 3D modeling and simulation tools facilitate improved product performance.

Inventor empowers users to create bespoke design configurations and automate routine tasks, resulting in time and cost savings. Additionally, Inventor's collaboration feature, which leverages an existing Autodesk account, is unmatched in the industry. By integrating their designs with customer data, users can work in a secure cloud environment that enables seamless collaboration.

3.3 Universal Laser System PLS 4.75

The PLS4.75 is a free-standing platform with a materials processing envelope of 24" x 18" x 8.5" or 3,672 in³ (610 x 457 x 216 mm or 60,214 cm³). The single laser platform supports either one 10.6µm CO2 laser (10 to 75 watts) or one 9.3µm CO2 laser (30, 50, or 75 watts).

Table 3.3: PLS 4.75 Specifications

Features	Parameters
Laser Materials Processing Area (W*H)	24*18 in
Maximum Part Size (W*H*D)	29 x 23 x 8.5 in
Compliance Voltage	+-30V
Overall Dimension (W x H x D)	36 x 39 x 36 in
Motorized Z Axis Lifting Capacity	40 lbs (18 kg)
Available Focus Lenses	2.0 in (51 mm) HPDFO™
Optics Protection	Integrated with included Gas Assist
Cabinet Style	Free-Standing
Laser Options	10, 30, 40, 50, 60 and 75 watts
Weight	270 lbs (122 kg)
Power Requirements	110V/10A 220V-240V/5A

3.3.1 Basic Working Principle of Co2 Laser System

Laser action is achieved in a molecular gas laser by transitions between vibrational and rotational levels of molecules. Its construction is straightforward, and its output is continuous. The transition between the vibrational states of carbon dioxide molecules occurs in the Co2 molecular

Table 3.4: PLS 4.75/Optimized Parameters for Engraving Sensor

Parameters	**Parameters**
Power	10 percent
Varied speed	5-10 percent
Pulse Per Inch	1000
z-axis	1 mm
Flow rate	250 CFM

gas laser. When there is an electric discharge in the gas, electrons collide with nitrogen molecules and are excited. Now, excited N2 molecules collide with ground-state CO2 atoms, exciting them to higher electronic, vibrational, and rotational levels. Because the excited level of nitrogen is so close to the E5 level of CO2, the population in the E5 level grows. When the population inversion is reached, any of the spontaneously emitted photons will activate the laser in the tube. There are two kinds of laser transitions.

1. Transition E5 to E4 will produce a laser beam of wavelength 10.6 μ m

2. Transition E5 to E3 will result in a laser beam with a wavelength of 9.6 μ m. Typically, the 10.6m transition is more intense than the 9.6m transition. This laser has a power output of 10kW.

3.4 Hauschild SpeedMixer SMART DAC 250

With the SMART DAC series, mixing is possible within a range of 250g to 1.5-2kg. Additionally, all models within the SMART DAC series are equipped with mixing volumes ranging from 310ml to 2.8 liters.

Table 3.5: Hauschild SpeedMixer SMART DAC 250 Specifications

Parameters	**Value**
Maximum mixing capability	250g
Maximum mixing volume	2800 mL
Mixing speed	350 to 2500 RPMs
Maximum mixing time	30 min

Figure 3.2: Hauschild SpeedMixer SMART DAC 250

3.5 NOVASCAN- Digital UV Ozone System

Ultraviolet Ozone Systems find extensive application in various industries such as electronics and semiconductors, as well as in research fields like biology, chemistry, physics, and materials science. The systems demonstrate remarkable efficiency in removing molecular organic impurities and preparing surfaces through the emission of intense ultraviolet light at 185 nm and 254 nm wavelengths. The presence of ambient oxygen leads to substantial O3 production and molecular excitation upon this emission. This unique combination facilitates the elimination of organic contamination at the molecular level on different substrates, including silicon, silicon nitride, glass, quartz, metals, and ceramics.

3.5.1 Basic Working Principle of UV Ozone System

An ozone generator, also known as an ozone machine, is a device designed to transform oxygen from various sources, such as ambient air, dry air, or concentrated oxygen, into ozone. These generators produce ozone (O3) by applying energy to oxygen molecules (O2), which leads to the separation of oxygen atoms and their temporary recombination with other oxygen molecules. The resulting ozone is utilized for water disinfection and air purification purposes.

Ozone generators work by applying an electrical charge to the air flowing through them. This process separates some oxygen atoms into unstable single atoms, which then bond with other oxygen molecules to create ozone. (Please note that the image is not to scale.)

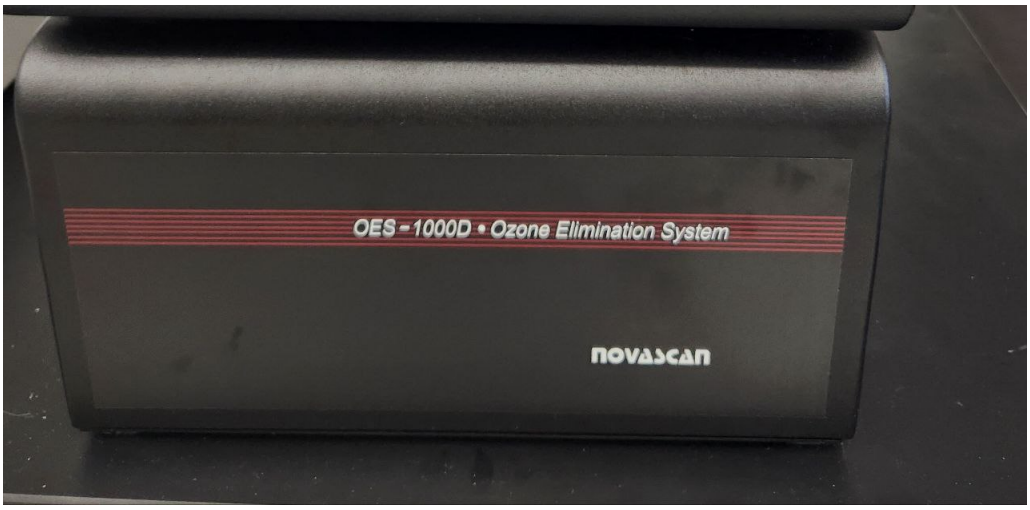

Figure 3.3: OES-1000D-Ozone Elimination System

Once generated, ozone reacts with pollutants, bacteria, viruses, or mold, breaking them down into simpler (and typically less harmful) molecules through a process known as oxidation. Unreacted ozone naturally decomposes back into oxygen over time. Ozonation is effective in eliminating odors and disinfecting air, water, and other substances. The USDA and FDA have even approved its use on food.

3.6 OES-1000D-Ozone Elimination System

The PSDP-UVT Pro series incorporates the advantages of both the PSD and PSDP UV systems and includes an additional PID-controlled heated sample stage that enables thermally-assisted UV treatment. These systems are highly useful for a diverse range of applications, including UV patterning, wafer cleaning, and thermal-enhanced UV curing.

The UV Ozone Cleaner effectively eliminates surface contamination from samples by utilizing a high-power UV light source to generate ozone. This process breaks down surface contaminants into volatile compounds that subsequently evaporate, leaving no residual trace. The Novascan PSDP-UV8T system features a high-intensity, low-pressure mercury vapor discharge lamp.

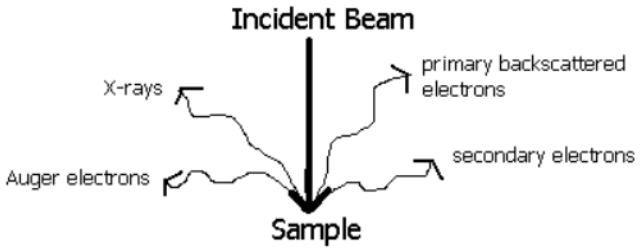

Figure 3.4: Working Principle of SEM

3.7 Scanning Electron Microscopy

3.7.1 Basic Working Principle of Scanning Electron Microscopy

The Scanning Electron Microscope (SEM) utilizes electrons, instead of light, to generate a significantly magnified image. An electron gun positioned at the top of the microscope generates a beam of electrons, which travels through a vacuum and follows a vertical path through the microscope. As the beam passes through electromagnetic fields and lenses, it is focused down toward the sample. Upon reaching the sample, the beam causes the emission of electrons and X-rays. The X-rays, backscattered electrons, and secondary electrons emitted from the sample are gathered by detectors and converted into an electronic signal, which is transmitted to a display screen resembling that of a television. The X-rays, backscattered electrons, and secondary electrons emitted from the sample are gathered by detectors and converted into an electronic signal, which is transmitted to a display screen resembling that of a television.

3.8 Sputtering System

3.8.1 Basic Working Principle of Sputtering System

Scanning Electron Microscopes (SEMs) have the capability to image an extensive range of sample types, such as semiconductors, metals and alloys, polymers, ceramics, and biological specimens. However, some samples can be challenging to image and require sputter coating to guarantee a high-quality image can be obtained.

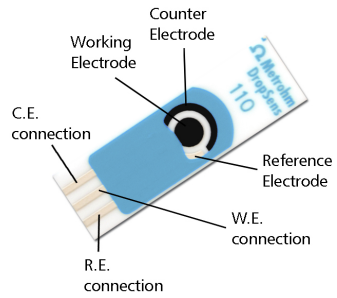

Figure 3.5: Screen Printed Carbon Electrode 110

The process of sputter coating involves placing the sample in a small, vacuum-sealed chamber, and using an electric field and argon gas to generate positive ions. These ions are attracted to a negatively charged gold foil, resulting in the displacement of gold atoms from the surface of the foil. These atoms then settle onto the surface of the sample, producing a thin coating of gold.

3.9 Screen Printed Carbon Electrode 110

Innovative strips designed for electrochemical analysis in environmental, clinical, or agri-food applications utilize screen-printed electrodes composed of inks containing carbon, gold, platinum, silver, or carbon nanotubes. These disposable devices are low-cost and intended for use with micro volumes of samples. They are ideal for both quality control and research purposes, as well as for teaching electrochemistry. The strips have general dimensions of 3.4 x 1.0 x 0.05 cm, and feature a reference electrode and electric contacts made of silver (unless otherwise specified).

Table 3.6: Metrohm Screen Printed Carbon Electrode 110 Specifications

Substrate material	Ceramic
Substrate size	3.4 x 1.0 x 0.05 cm
WE material	Carbon
AUX material	Carbon
REF material	Silver
WE diameter (mm)	4
WE geometric area (cm2)	0.11
MultiAnalysis Configuration	NO
IDE Band/Gap dimensions	NO

CHAPTER IV

FABRICATION

4.1 Laser Engraved Kapton Sensor

The direct induction of graphene formation through a carbonization process can also be achieved by exposing special polymeric materials to laser irradiation. A recent study used a CO2 laser to induce graphene formation from a PI substrate under ambient conditions. The localized temperature increase caused by the laser (>2500°C) leads to carbonization on the surface of the PI, where C-O, C=O, and N-C bonds in the PI network are broken down and the aromatic compounds rearrange to form graphitic structures. The PI film changes colour from light orange to black after the laser treatment. Laser-induced graphene (LIG) offers several advantages over other methods such as chemical vapor deposition (CVD) for creating graphene patterns. LIG eliminates the need for a complex substrate-transfer process and allows patterns to be written directly without masks. These advantages make LIG a popular choice for producing flexible electronics, including sensors and supercapacitors. However, the quality of LIG may still be inferior to that of pristine graphene

Figure 4.1: Kapton polyamide film

Figure 4.2: Sensor After Laser Engraving

produced through mechanical exfoliation from graphite. .

4.1.1 Engraved the Electrode by Universal Laser System

The pattern was engraved on Kapton foil using a Universal® Laser System (PLS 4.75 (60 W) 10.6μm CO2 laser).

Step01: Before engraving, the 127-micrometre-thick Kapton films were rinsed in alcohol for 15 minutes to remove impurities, washed repeatedly with DI water, and left to naturally dry.

Step 02: The Kapton foil was then cut into appropriately sized sheets, and the borders were taped directly onto the engraving table of the machine.

Step03: To optimize the laser system parameters, we had to consider the resistance of the laser-engraved Kapton electrode, which heavily depends on the charge transfer rate of the electrodes. Therefore, we used 10 per cent power, a varied speed of 5-10 per cent, 1000 Pulse Per Inch (PPI), and a 1 mm z-axis specification to achieve optimal electrode patterning. It is important to note that direct conversion to physical units may be inappropriate in some cases, as percent power and measured power scale are linearly only approximately. The machine software provided the desired PPI in both directions. At the same time, the air was continuously extracted from the scribing chamber during the operation time with an exhaust flow rate of 250 CFM to remove soot and other gases.

Step 04: We made the reference electrode and contact pad with silver ink and left it dry for 24 hours.

Table 4.1: Kapton Sensor Size Parameters

Features	Parameters
Length	3.4 cm
Width	10 cm
Height	0.05 cm
Working Electrode Diameter	4 mm

4.2 Preparation of Graphene-Conductive Inks

The use of conductive inks has surfaced as a promising and innovative approach to enhance the manufacturing processes of electronics. Employing these inks makes it feasible to produce printed electronic devices that offer significant benefits compared to traditional silicon-based electronic devices.

Conductive inks comprise conductive materials suspended in a suitable solvent or mixture of solvents, accompanied by stabilizers such as binder agents, surfactants, or polymers. In addition to exhibiting high electrical conductivity, these inks should possess characteristics such as low viscosity, good stability, printability, and adhesion to diverse types of substrates, while being affordable and easy to prepare. It is also essential that the conductive ink retains its electrical conductivity and chemical inertness throughout the printing and post-printing processes, and dries compactly on the substrate to create a uniform and adherent conductive film. Furthermore, with the growing popularity of wearable electronics and bioelectronics devices, biocompatibility has become an increasingly valuable attribute for conductive inks.

4.2.1 Materials

Graphene nanoflakes (2-10 nm thickness, diameter approximately 5 m, 8000S/m Conductivity,20 to 40 m2/g specific surface area and 5 GPa tensile strength), Poly(3,4-ethylene dioxythiophene)-poly(styrene sulfonate) (PEDOT:PSS), Polyaniline, Phytic acid, Dimethyl Sulfoxide (DMSO), Potassium hexacyanoferrate(III), Reagent Plus, 99 percent Potassium hexacyanoferrate(II) trihydrate, silver ink were purchased from Sigma-Aldrich (Figure 5.2).

Figure 4.3: Materials for Graphene Conductive Ink

Figure 4.4: Graphene conductive pedot:pss ink

4.2.2 G-PEDOT: PSS Ink

To prepare the conductive PEDOT: PSS ink with graphene, a mixture of 1 gm of graphene nanoflakes, 0.1 gm of PEDOT: PSS, 800 L of DMSO, and 6 ml of DI water was utilized. DMSO was incorporated to enhance the ink's conductivity, given that PEDOT: PSS exhibits low conductivity (1 S/cm) and hydrophilicity. We have used Hauschild SpeedMixer SMART DAC 250 for homogenous solutions of ink.

4.2.3 G-PANI ink

The preparation of graphene conductive Polyaniline ink involved combining 1gm of graphene nanoflakes with 2 mL of Polyaniline, 4 mL of phytic acid, and 6 mL of DI water. Phytic acid was chosen as the medium for ink preparation because the conductivity of polyaniline is elevated in an

Figure 4.5: Graphene conductive polyaniline ink

Figure 4.6: Working Electrode Modification With Graphene Conductive Ink

acidic environment. The same above process has been followed.

4.3 Electrode Modification with Graphene Inks

The surface modification of the electrode is crucial to the performance of biosensors, given the functional mechanism of these devices. To enhance the performance of the proposed biosensor, we have modified the working electrode area of the scree-printed and laser-engraved biosensors with G-PEDOT: PSS and G-PANI ink.

We have used 2 μL pipet, covered the working electrode area with the proposed inks and dried overnight naturally.

Figure 4.7: PDMS-Elastomer Base & Curing Agent

4.4 PDMS Preparation

We have prepared Polydimethylsiloxane (PDMS), to protect the sensor from being highly resistive during ozonolysis. The following steps are given for PDMS preparation:

Step 01: We have prepared a mixture of Sylgard 184 silicone elastomer base and curing agent with 10:1 ratio by mass.

Step 02: After mixing the solutions, they were placed inside a vacuum chamber for 10 minutes.

Step 03: The resulting mixture was pasted between the working area, and the contact path. Then the sensor was left to dry for 24 hours.

4.5 Immune Sensor Preparation

The preparation of immune sensors is a critical aspect of biosensor development, enabling the detection and quantification of specific biological molecules. Immune sensors are based on the principle of immunoassays, which use antibodies to recognize and bind to specific antigens, triggering a signal that can be detected and measured. To prepare immune sensors, various

Figure 4.8: IL-6 antibody

techniques can be employed to immobilize antibodies on the sensor surface, including physical adsorption, covalent attachment, and layer-by-layer deposition. The choice of immobilization method can significantly impact the sensor's sensitivity, specificity, and stability. Additionally, optimizing the concentration of immobilized antibodies, buffer pH, and blocking agents is essential for enhancing the sensor's performance.

Step 01: We have coated the LEK/G-PANI electrode with the thin PDMS layer between the electrode and contact pads.

Step 02: We have ozonolysis the sensor for 60 sec using Novascan Ozone Instrument to introduce -COOH- layer on the electrode surface.

Step 03: 0.4 M EDC was added to the electrode surface area and kept the sensor in a dark environment for 2 hours.

Step 04: 0.4 M NHS was added to the electrode surface area and kept the sensor in a dark environment for another 2 hours.

Step 05: After that we added 2 μL of antibody to the electrode surface and kept the sensor in a dark environment for another 24 hours.

4.6 Sensor Interface With Autolab Potentiostat

The interface between a sensor and an Autolab potentiostat is critical for electrochemical measurements and analysis. The Autolab potentiostat provides a platform for precise control of the potential at the working electrode and measurement of the resulting current. To interface the sensor with the potentiostat, the sensor must be connected to the appropriate input ports, and the

potentiostat settings must be adjusted to suit the desired measurement parameters. These settings include the applied potential range, scan rate, and data acquisition rate. Additionally, software programs (Nova) can be used to automate the measurement process and analyze the resulting data. The successful interface between a sensor and an Autolab potentiostat is essential for reliable and accurate electrochemical measurements and analysis.

We fabricated the laser-engraved sensor with the same dimension as the screen-printed electrode, and then we connected the laser-engraved kapton sensor with the same port that we got from Metrohm.

CHAPTER V

RESULT & DISCUSSION

5.1 Characterization of Graphene-Conductive Inks

5.1.1 SEM Characterization

SEM was utilized to characterize the flake size, microstructure of graphene-like materials, and morphology of graphene conductive G-PEDOT:PSS and G-PANI ink patterns. The morphological characteristics of G-PEDOT:PSS ink are depicted in Figure 6.1. The microstructure analysis reveals a rough structure of G-PEDOT:PSS, with an average nanoparticle size of approximately 60 nm (at 40,000x magnification). The coexistence of graphene and PEDOT: PSS indicates a molecular binding between the two components.

SEM images in Figure 6.2 display the microstructure of G-PANI ink, which exhibits a smoother surface compared to G-PEDOT:PSS ink. Consequently, G-PANI ink displays stronger binding with the working electrode. SEM analysis also reveals the presence of roughness in the PANI layer, with a nanoporous structure of approximately 1 μm diameter observed at 40,000x

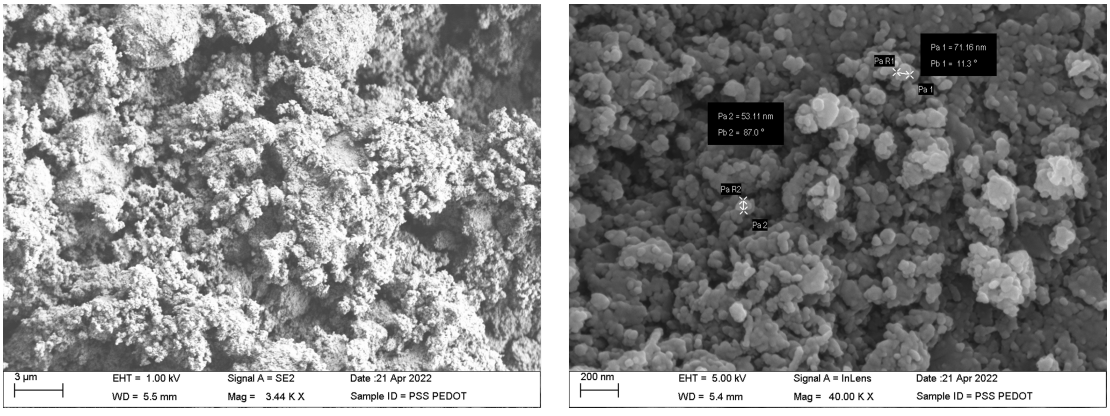

Figure 5.1: SEM characterization of G-PEDOT:PSS ink

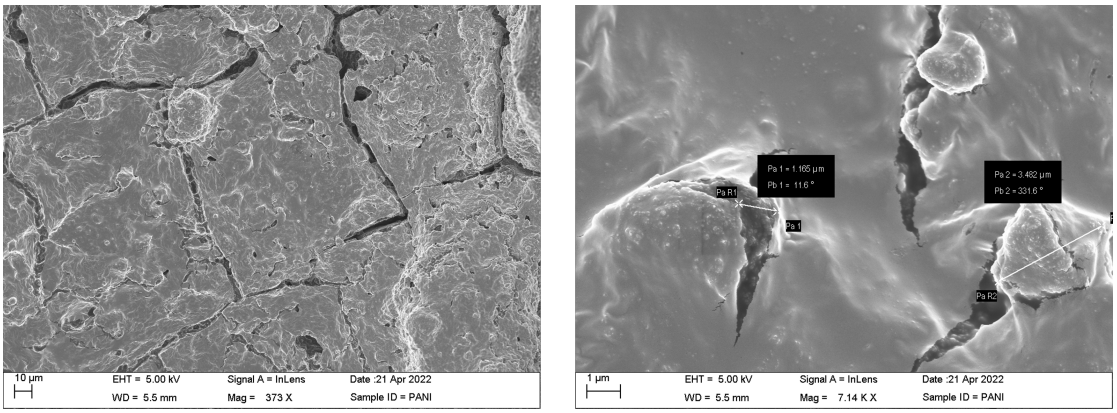

Figure 5.2: SEM characterization of G-PANI ink

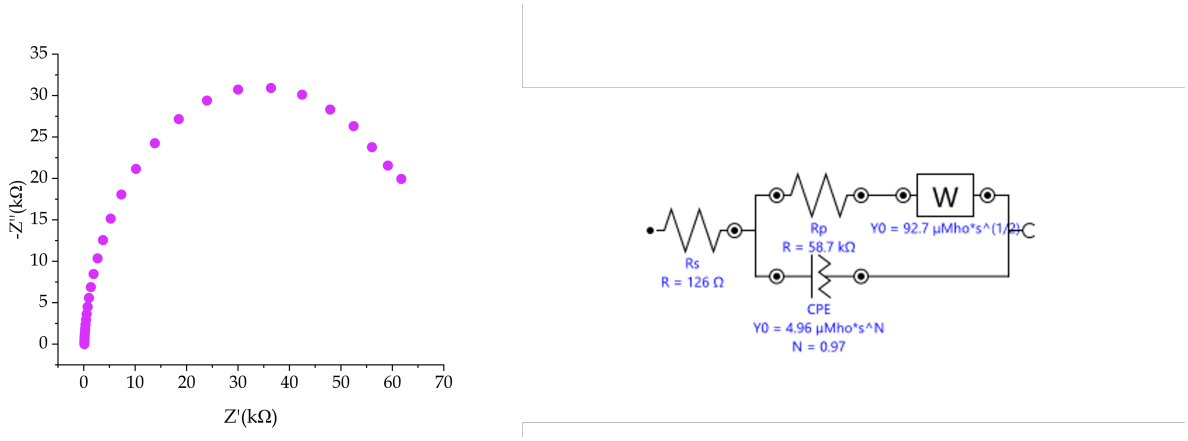

Figure 5.3: EIS & Equivalent Circuit of Bare SP

magnification.

5.1.2 EIS Characterization of Graphene Conductive Inks

The interfacial properties of the inks were evaluated and compared to those of commercial screen-printed electrodes using electrochemical impedance spectroscopy (EIS). The Nyquist spectrum typically consists of a low-frequency zone that pertains to the diffusion process and a high-frequency region corresponding to electron transfer. In Figure 1, the Nyquist plots (frequency range: 10^6 to 10 Hz) display nearly perfect semicircles, which are indicative of non-diffusion-limited electrochemical processes.

The diameter of the Nyquist semicircle is largely determined by the charge transfer resistance (Rct) and decreases as the conductivity of the electrode surface increases, resulting in a shift towards

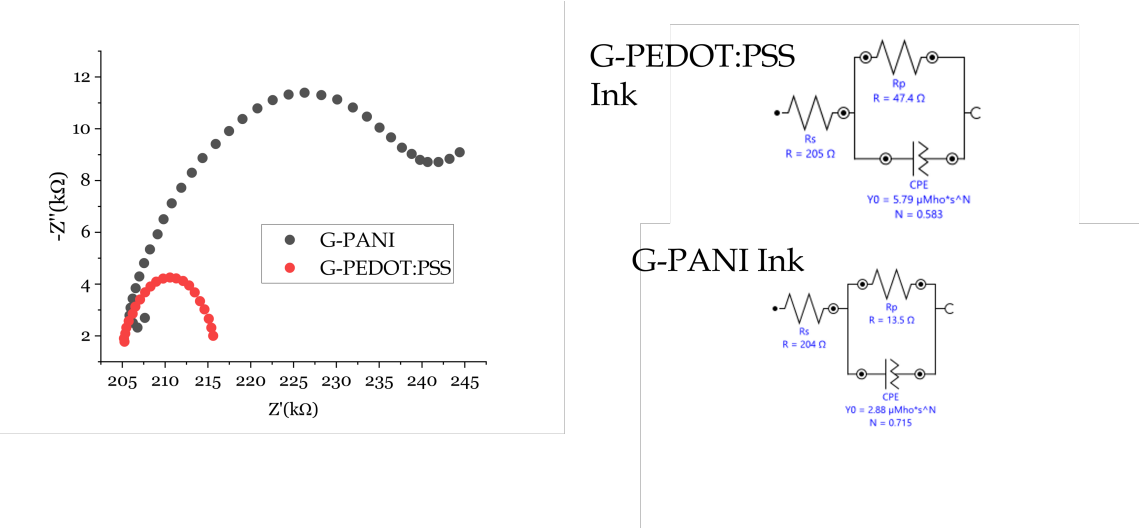

Figure 5.4: EIS & Equivalent Circuit of G-PEDOT and G-PANI inks

lower Rct values. This trend can be explained by a simpler equivalent circuit model that does not incorporate diffusion-associated impedance.

The lowest Rct value was observed for G-PANI ink (13.5 ohm) compared to G-PEDOT:PSS ink (47.4 ohm) and commercially available bare screen-printed electrode (58.7 kohm). The lowest Rct value of G-PANI ink indicates that PANI is a highly conductive polymer, has a large surface area, and high redox activity and stability contributing to the efficient electron transfer at the electrode-electrolyte interface. The nonlinear shape of the Nyquist plot for G-PANI ink (Figure) may be attributed to ion transport limitation in the electrolyte within the porous electrode structure.

5.2 Characterization of LEK Electrodes

5.2.1 Reproducibility

The biosensor's capacity to produce identical responses in a duplicated experimental setup is referred to as reproducibility, which is determined by the transducer and electronics' precision and accuracy. Precision measures the ability of the sensor to yield consistent results when a sample is measured multiple times, whereas accuracy determines the sensor's ability to provide a mean value close to the true value upon repeated sample measurements. A biosensor with reproducible signals ensures high reliability and robustness of the conclusions drawn from its response. The

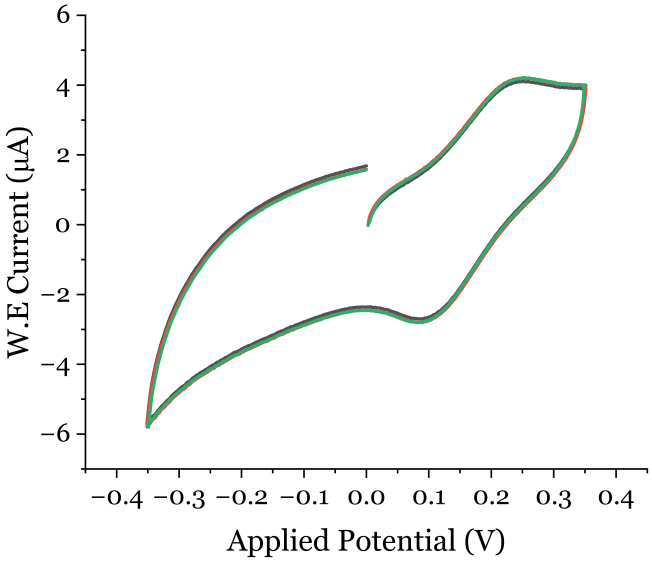

Figure 5.5: Reproducibility of LEK Electrodes from four different fabrication batches

reproducibility of the fabrication was assessed using four distinct laser-induced Kapton sensors, as shown in Figure 5.5. The analytical response exhibited a consistent relative standard deviation (RSD) of 1.01% for Ip values with a sample size of n=4.

5.2.2 Repeatability

The repeatability of a biosensor refers to the ability of the biosensor to produce identical responses when a single sample is measured multiple times. It is a measure of the biosensor's precision and is determined by the variation in the output signals of repeated measurements of the same sample. A biosensor with high repeatability will produce consistent results and is essential for accurate and reliable measurements. The stability of the electrochemical response was evaluated during the experiments by conducting five cyclic voltammograms with a scan rate of 0.08 V/sec using the same electrode, as depicted in Figure 5.6 . The results demonstrate excellent repeatability, with a relative standard deviation (RSD) of 0.76% for Ip values with a sample size of n=5.

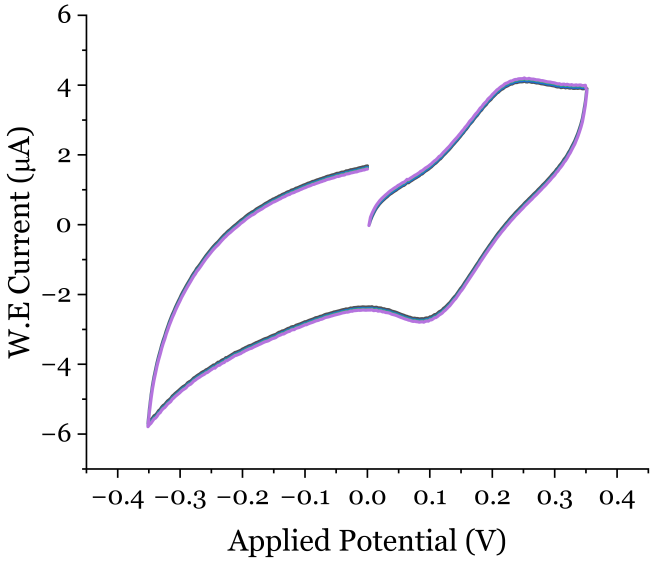

Figure 5.6: Repeatability of LEK Electrodes from five sensors of same fabrication batche

5.2.3 Bending

The storage stability of a biosensor is an important consideration for its practical application, as it determines the shelf life of the sensor and its ability to produce consistent results over time. In this context, the stability of the laser-engraved Kapton sensor was evaluated by subjecting it to repeated bending. The results showed that the fabrication process of the sensor was highly stable, with a relatively small RSD value of 4.39% for Ip values, indicating that the sensor was able to provide consistent results even after repeated bending.

Furthermore, the anodic peak current of the sensor slightly increased after bending, followed by a decrease after 10 bendings. However, after 12 bendings, there was no change observed in the peak current, suggesting that the sensor had reached a stable state. These findings indicate that the laser-engraved Kapton sensor has a high degree of stability, which is crucial for its use in practical applications.

5.2.4 Control Experiment

A control experiment in biosensor is an experiment in which all the variables are kept constant except for one, which is the variable being tested. The purpose of a control experiment is

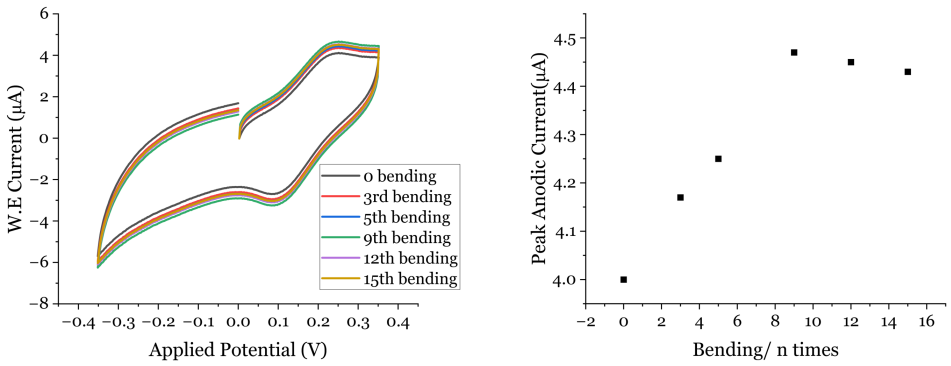

Figure 5.7: Repeatative bending & linear plot

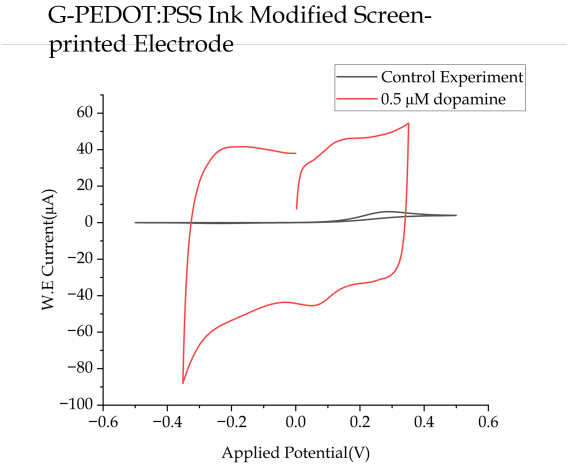

Figure 5.8: Control Experiment of G-PEDOT:PSS/SPE

to provide a baseline or a reference point to which the results of the variable being tested can be compared.

In the case of a biosensor, a control experiment may involve measuring the response of the biosensor in the absence of the analyte (i.e., the molecule of interest that the biosensor is designed to detect). This can help to establish the baseline response of the biosensor and to ensure that any changes in response are due to the presence of the analyte rather than other factors such as environmental changes or instrument drift. In our control experiment, we have done the testing on screen-printed electrodes (G-PEDPT:PSS and G-PANI modified)with redox couples with and without dopamine. With only a redox couple. no prominent peak was observed. But in presence of dopamine, prominent oxidation and reduction peak was observed in cyclic voltammogram due to

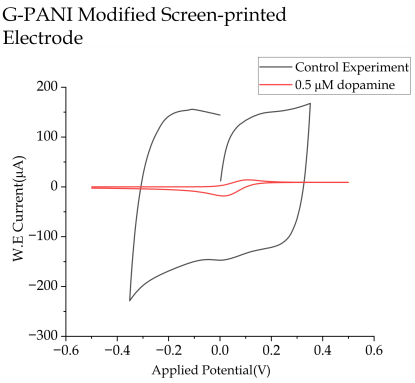

Figure 5.9: Control Experiment of G-PANI/SPE

the oxidation of dopamine to dopamine -o-quinone.

5.3 Electrochemical Performance Evaluation of LEK Electrodes in Dopamine Detection

The unmodified and modified electrodes' effective surface area (Aeff) was determined using the Randles-Sevcik linear equation, which relates the anodic current peak to the scan rate of 0.08 V/sec.

$$I_p = 0.4463 \left(\frac{F^3}{RT}\right)^{1/2} n^{3/2} A_{eff} D^{1/2} C_v^{1/2} \tag{5.1}$$

In this study, Ip represents the anodic peak current measured in amperes, while n refers to the number of mole electrons transferred during the redox reaction. F represents the Faraday constant, Aeff is the effective surface area of the electrode measured in cm², C is the concentration of dopamine measured in mol/cm³, D is the diffusion coefficient of dopamine (7.38 × 10 cm²/s), v is the scan rate measured in V/s, R represents the gas constant, and T represents temperature measured in Kelvin.

For the Kapton sensor, the effective surface area of the bare, G-PEDOT: PSS, and G-PANI ink-modified sensors were found to be 0.78, 1.76, and 4.59 mm², respectively.

5.3.1 Sensitivity

In order to assess the electrocatalytic performance of the suggested G-PEDOT:PSS and G-PANI inks, modifications were made to LEK electrodes. The cyclic voltammograms (CV) of the modified screen-printed and Kapton electrodes using the proposed inks, in the presence of 0.5 µM dopamine and Fe2+/Fe3+ redox couples in a basic medium (PH=7.4), are illustrated in

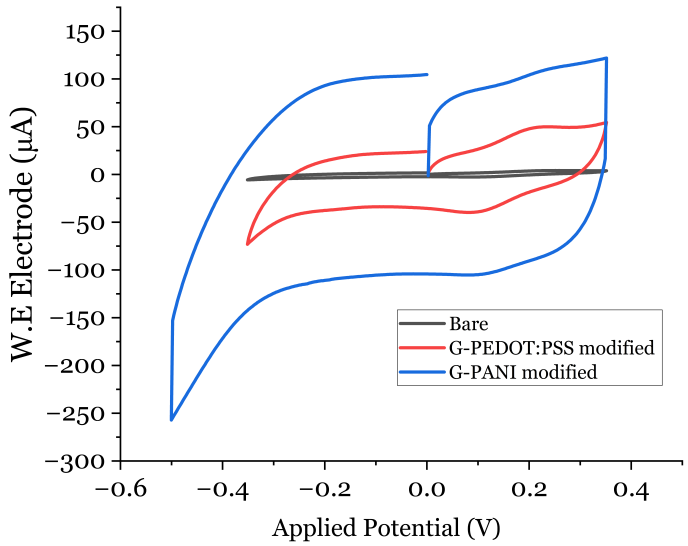

Figure 5.10: Performance comparison between bare, G-PEDOT:PSS & G-PANI ink LEK electrode

Figure. The anodic peak currents are 4.08 μA, 49.26μA, and 107.25μA respectively for LEK, LEK/G-PEDOT:PSS and LEK/G-PANI electrodes. The higher anodic peak current indicates a higher concentration of the analyte and a more rapid oxidation reaction at the electrode surface.

The observed increase in anodic peak current from LEK to LEK/G-PEDOT:PSS to LEK/G-PANI electrodes can be explained by the following reasons:

1. **Increased electroactive surface area**: The addition of conductive polymers such as PEDOT:PSS and PANI onto the LEK electrode surface can increase the surface area available for electrochemical reactions. This increase in surface area can lead to an increase in the number of available sites for oxidation, resulting in higher peak currents.

2. **Improved electron transfer rate**: Conductive polymers such as PEDOT:PSS and PANI can facilitate electron transfer between the electrode and the solution. This improved electron transfer rate can result in faster oxidation reactions and higher peak currents.

3. **Enhanced electrocatalytic activity**: PEDOT:PSS and PANI can act as electrocatalysts, facilitating the oxidation of the electroactive species. This can result in a more efficient electrochemical reaction and higher peak currents.

We have further calculated ∇Ep of the LEK, LEK/G-PEDOT:PSS and LEK/G-PANI electrodes respectively 139 mV, 127 mV, 120 mV. The ∇Ep is related to the activation energy of the electrochemical reaction and can provide information about the reaction mechanism. A smaller peak separation indicates a more facile electron transfer and a faster reaction kinetics, whereas a larger peak separation indicates a slower reaction kinetics or a more complex reaction mechanism.

5.3.2 Limit of Detection of Dopamine

The limit of detection (LoD) is characterized as the minimum quantity or concentration of a component that can be accurately distinguished from the limit of blank (LoB). This value determines the analyte level at which the probability of a low-level sample generating a false-negative result is equivalent to the predetermined Type II error risk. Typically, the Type II error risk is set at 0.05, which is the same as that used for Type I error risk. A parametric method is utilized to determine the LoD, assuming that the measurement variability of low-level samples follows a reasonable Gaussian distribution.

$$LOD = 3\frac{S_b}{m} \tag{5.2}$$

Here, Sb is the standard deviation between the blank signal, m is the slope of the calibration curve and 3 is the signal-to-noise ratio.

The anodic peak current and dopamine concentrations have a linear relationship. We have calculated Ipa over the range of 0.5 μM to 5 μM dopamine for LEK, LEK/G-PEDOT:PSS, and LEK/G-PANI electrodes. The LOD for LEK, LEK/G-PEDOT:PSS, and LEK/G-PANI electrodes are respectively 1.441μM, 0.567 μM, and 0.4084 μM.

5.4 Comparison With Commercially Available Electrodes

This study compared the sensitivity and limit of detection (LOD) of laser-engraved Kapton sensors with the commercially available screen-printed sensors from Metrohm, using G-PEDOT:PSS and G-PANI inks. We found that the redox peak current for both G-PEDOT:PSS and G-PANI ink on the screen-printed electrode (SPE) was significantly higher compared to bare SPE, with increases of 16.55 and 41.47 times, respectively (Figure 5.12).

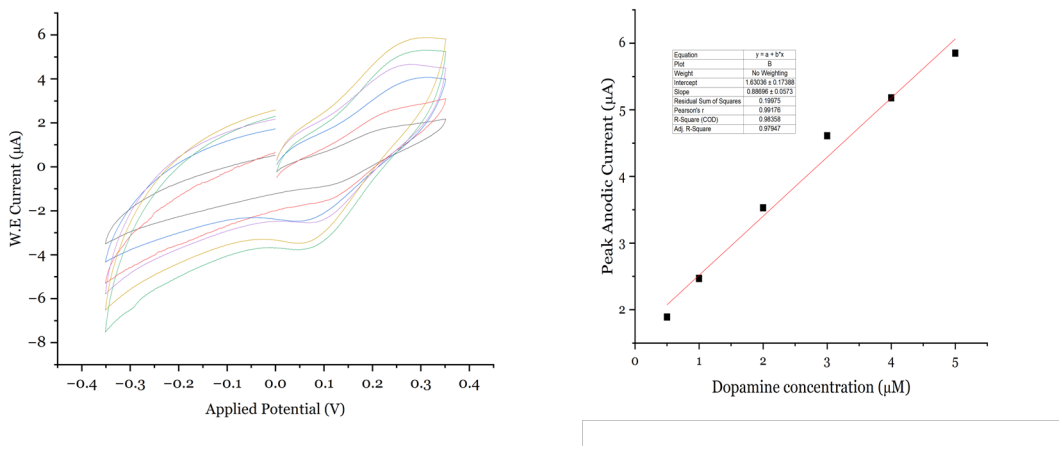

Figure 5.11: Different Concentrations of dopamine in bare kapton & linear plot

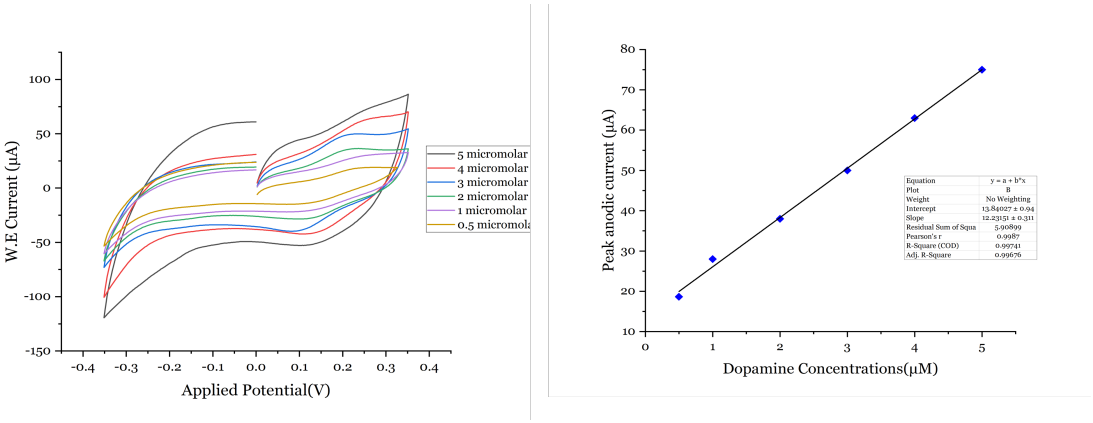

Figure 5.12: Different Concentrations of dopamine in LEK/G-PEDOT & linear plot

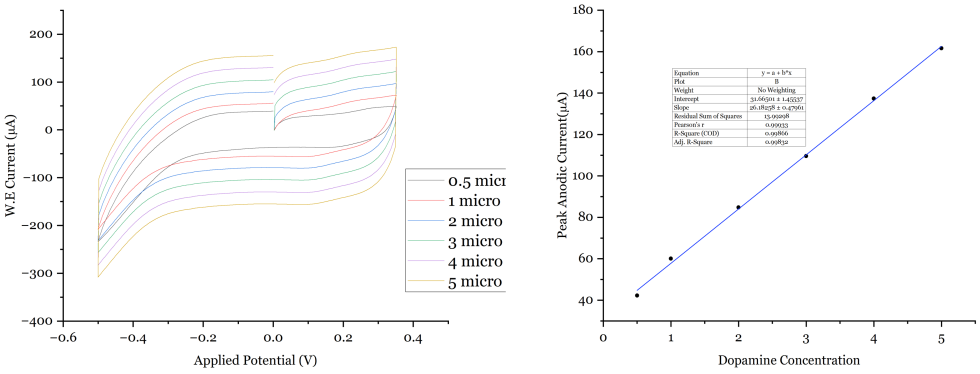

Figure 5.13: Different Concentrations of dopamine in LEK/G-PANI & linear plot

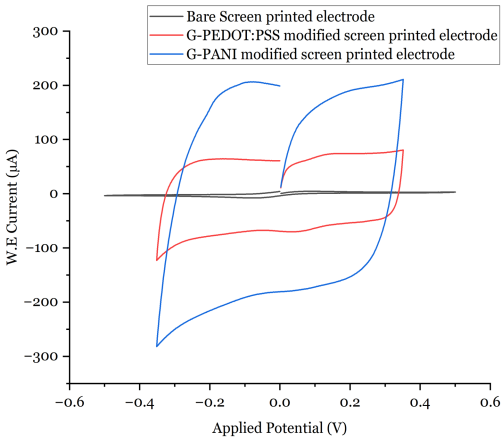

Figure 5.14: Screen-Printed Electrode Sensitivity

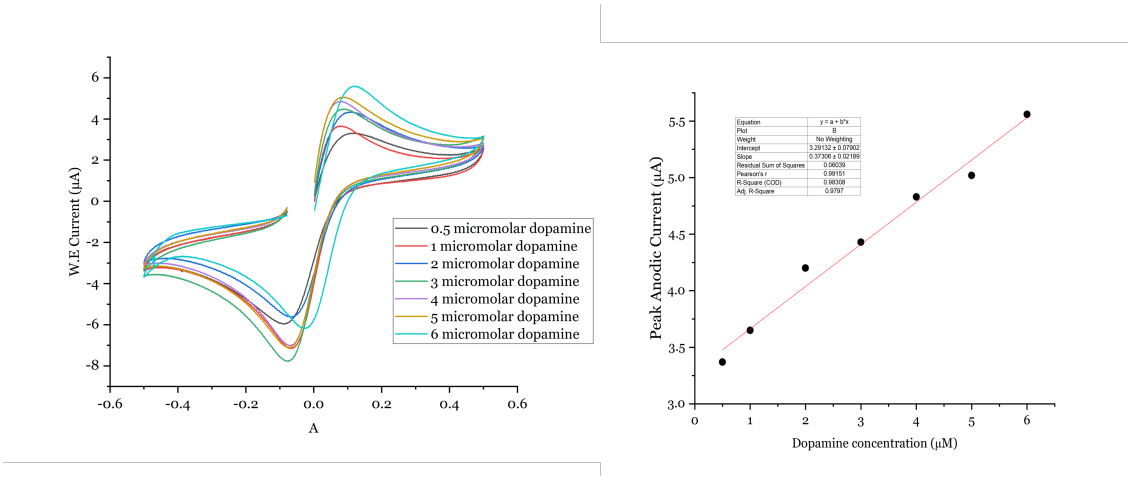

Figure 5.15: Different Concentrations of dopamine in bare sp & linear plot

Additionally, when compared to the laser engraved Kapton sensor, the G-PANI ink (LEK/G-PANI) showed the highest peak current, with approximately 22.17 times greater than LEK, and the G-PEDOT:PSS ink (LEK/G-PEDOT:PSS) showed 20.91 times greater than LEK. This indicates that the laser-engraved Kapton sensor is more sensitive to these inks, with higher redox peak currents observed.

Furthermore, our results revealed that the screen-printed electrode had a higher LOD compared to the laser-engraved Kapton sensor. A table is given below for the LOD of screen-printed electrodes:

This implies that the laser-engraved Kapton sensor is capable of detecting lower concen-

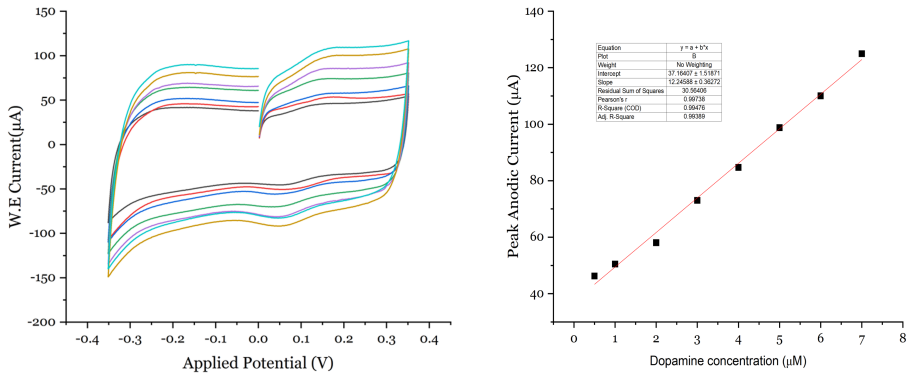

Figure 5.16: Different Concentrations of dopamine in bare G-PEDOT:PSS/SPE & linear plot

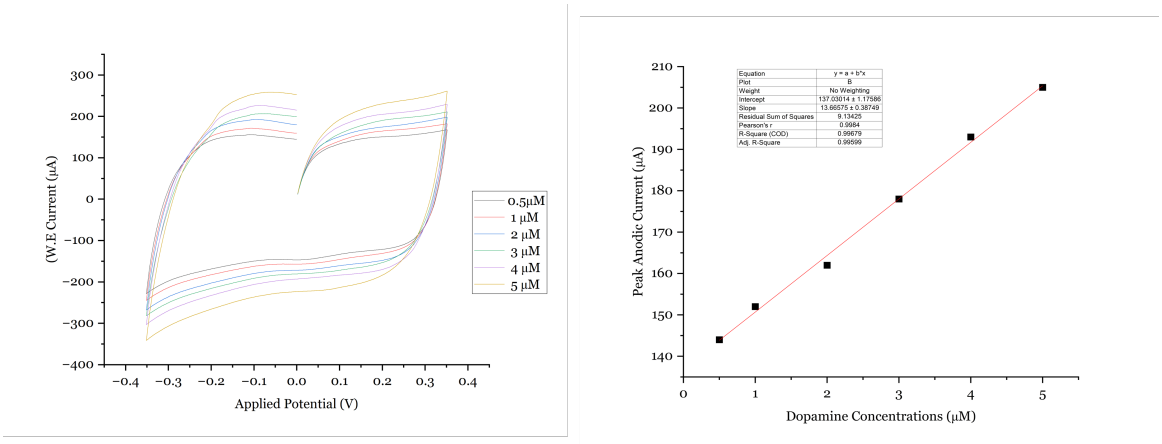

Figure 5.17: Different Concentrations of dopamine in G-PANI/SPE & linear plot

Table 5.1: Sensor Size Parameters

Features	Parameters
SPE	1.974 μM
SPE/G-PEDOT:PSS	0.867μM
SPE/G-PANI	0.632 μM

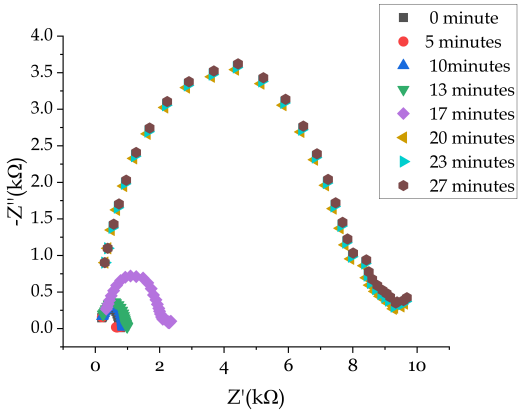

Figure 5.18: Stability check of IL-6 sensor

trations of the analyte of interest, making it a more sensitive analytical tool compared to the screen-printed electrode.

5.5 IL-6 Immune Sensing

In this study, we investigated the analytical performance of an engineered biosensor based on LEK/G-PANI for the detection of IL-6 antigen using Electrochemical Impedance Spectroscopy (EIS) techniques under optimal analysis conditions. The sensor was modified by ozonolysis to introduce carboxyl anion (–COO) groups on the sensor surface, which led to a significant increase in the diameter of the semicircle in the EIS. This modification inhibited the electron transfer between the modified electrode and the negatively charged redox species.

After further coating the LEK/G-PANI electrode with an IL-6 antibody, a second semicircle appeared in the EIS, with a larger charge transfer resistance (Rct) value. This indicated that the anti-IL-6 antibody had successfully immobilized on the electrode, forming a hybrid IL-6 antibody film that acted as a kinetic barrier for the electron transfer of the redox marker (Figure 5.17). To detect IL-6 antigen, we drop cast the antigen on the working electrode area and waited for

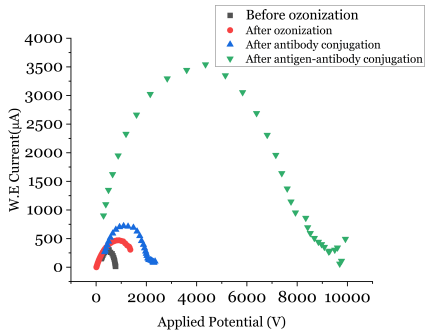

Figure 5.19: Signal Changes in Immune Sensor Preparation

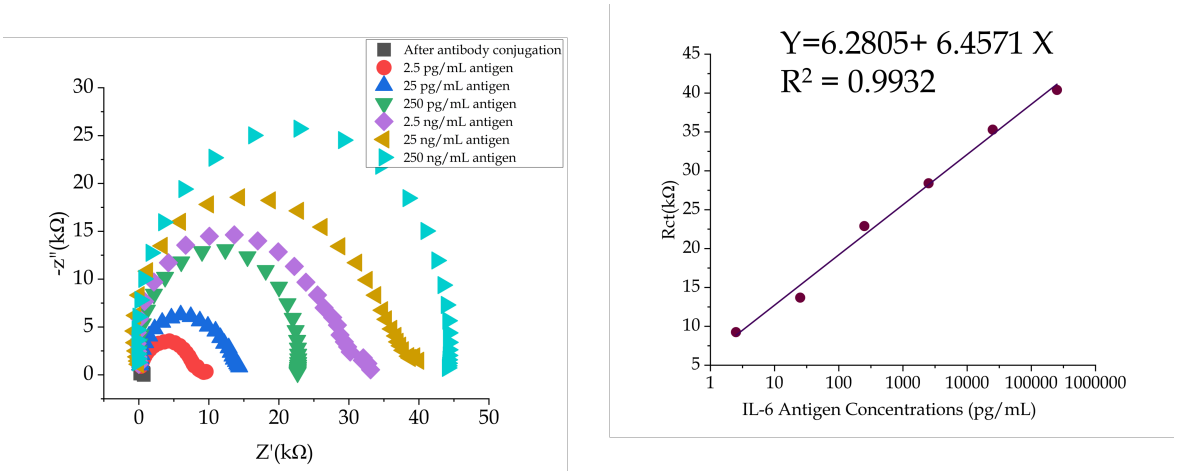

Figure 5.20: LOD of IL-6 sensor

20 minutes to obtain a stable signal (Figure 5.16). Interestingly, an increase in Rct value was observed after binding with IL-6 antigen, indicating that the IL-6 antigen further increased the charge transfer resistance of the biomarker (Figure 5.18). We observed a well-defined concentration dependence curve for IL-6 antigen, with a linear relationship between the ∇Rct and the IL-6 antigen concentrations within a range of 2.5 pg/mL to 250 ng/mL. The regression equation for the relationship was ∇Rct = 6.2805 + 6.4571 (IL-6 concentrations) (R2=0.9932) with LOD 2.6234 pg/mL, which is significantly lower than the level of IL-6 in human body (10–12 pg/mL). These results showed that the amount of bound IL6 antigen increased as IL6 concentration increased, forming a protein layer that served as a nonconductive barrier and inhibited electron transmission.

The repeatability of the sensor was evaluated, and the error bars were shown in the supplementary figure (). Table 2 compared the LOD performance of our studied electrodes with some other

electrodes for IL-6 immune sensing. Our LEK/G-PANI biosensor exhibited a lower LOD (2.6234 pg/mL) and more sensitivity compared to other biosensors. Very small amounts of chemicals were needed for the fabrication process, and the fabrication steps were simple. Therefore, we can conclude that the fabricated LEK/G-PANI sensor is fast, reliable, and environmentally friendly for IL-6 detection.

5.5.1 Detection of IL-6 in human serum sample

Detecting IL-6 in human serum samples is a crucial step towards developing a practical diagnostic tool for various diseases, including cancer and autoimmune diseases. To detect IL-6 in serum samples, the biosensor can be used to measure the amount of IL-6 present in the sample. However, detecting IL-6 in serum samples poses several challenges due to the complex matrix of serum samples, which contains a variety of proteins, lipids, and other biomolecules that can interfere with the biosensor's response.

We have detected IL-6 in human serum (Heat Inactivated, from human male AB plasma, USA origin, sterile-filtered, purchased from Sigma Aldrich). We have used 2μL of 2 pg/ml, 200 ng/ml, and 20μg/ml concentrations of IL-6 in 10μL in human serum samples(Figure 5.19. The diameter of the EIS semicircle increases after adding IL-6 antigens to the human serum sample Tas the formation of this complex creates a non-conductive barrier that inhibits the electron transfer between the modified electrode and the negatively charged redox species. This increase in impedance results in the observed increase in the diameter of the EIS. The increase in diameter is indicative of a larger charge transfer resistance (Rct) value, which reflects the binding of IL-6 to the biosensor surface.

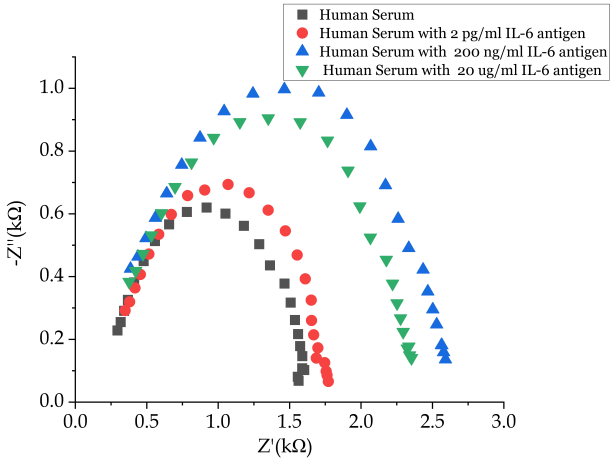

Figure 5.21: Detection of IL-6 in human serum sample

CHAPTER VI

CONCLUSION

6.1 Conclusion

A stretchable highly sensitive laser-induced graphene bio and the immune sensor has been developed to detect dopamine and IL-6. By modifying the electrodes with graphene-based conductive inks, the proposed sensors performed excellently with high sensitivity and lower LOD. We have first reported the G-PANI ink , which is 41.47 times more sensitive compared to the bare SPE. We can further extend our work to detect environmental estrogen and other proteins.

6.2 Future Work

Optimization of electrode coatings: We will further investigate other conductive ink materials, such as graphene oxide or carbon nanotubes, and their effects on electrode performance. We will also explore different ratios of the graphene conductive ink and the conducting polymer used for the electrode coatings, as well as different thicknesses of the coating layers.

Real-world application: We will explore the real-world application of these electrodes. This can include testing the electrodes in various physiological media, such as blood or saliva, to evaluate their performance in detecting dopamine and IL-6 levels in vivo. Furthermore, the integration of these electrodes into wearable or implantable devices can be explored.

Comparison with other electrode materials: We will compare the performance of these electrodes with other commercially available electrodes, such as carbon fiber electrodes or gold electrodes. This can be done by evaluating their sensitivity, LOD, and response time.

Biosensing applications: We will focus on exploring other biosensing applications for these electrodes. This can include detecting other neurotransmitters or biomolecules, such as glucose or

lactate, or developing biosensors for disease diagnosis or monitoring.

Overall, these future works can provide insights into the optimization and application of these novel LEK electrodes modified with graphene conductive inks, and pave the way for their practical use in wearable and stretchable bioelectronics applications.

REFERENCES

[1] K. L. ADAMS, M. PUCHADES, AND A. G. EWING, *In vitro electrochemistry of biological systems*, Annu. Rev. Anal. Chem., 1 (2008), pp. 329–355.

[2] S. AKIRA, T. TAGA, AND T. KISHIMOTO, *Interleukin-6 in biology and medicine*, Advances in immunology, 54 (1993), pp. 1–78.

[3] A. A. BALANDIN ET AL., *Superior thermal conductivity of single-layer graphene*, Nano letters, 8 (2008), pp. 902–907.

[4] G. BOLT, *Analysis of the validity of the gouy-chapman theory of the electric double layer*, Journal of Colloid Science, 10 (1955), pp. 206–218.

[5] A. W. BOTT, *A comparison of cyclic voltammetry and cyclic staircase voltammetry*, Current Separations, 16 (1997), pp. 23–26.

[6] A. BROWN AND S. GERSHON, *Dopamine and depression*, Journal of Neural Transmission/General Section JNT, 91 (1993), pp. 75–109.

[7] L. Y. CHEN ET AL., *Assessing the importance of interleukin-6 in covid-19*, The Lancet Respiratory Medicine, 9 (2021), p. e13.

[8] P. CLAUWAERT, P. AELTERMAN, T. H. PHAM, L. DE SCHAMPHELAIRE, M. CARBALLA, K. RABAEY, AND W. VERSTRAETE, *Minimizing losses in bio-electrochemical systems: the road to applications*, Applied microbiology and biotechnology, 79 (2008), pp. 901–913.

[9] R. M. CROOKS, *Principles of bipolar electrochemistry*, ChemElectroChem, 3 (2016), pp. 357–359.

[10] D. R. CROW, *Principles and applications of electrochemistry*, CRC Press, 1994.

[11] R. DE MARCO, G. CLARKE, AND B. PEJCIC, *Ion-selective electrode potentiometry in environmental analysis*, Electroanalysis: An International Journal Devoted to Fundamental and Practical Aspects of Electroanalysis, 19 (2007), pp. 1987–2001.

[12] M. DERVISEVIC, M. SENEL, AND E. CEVIK, *Novel impedimetric dopamine biosensor based on boronic acid functional polythiophene modified electrodes*, Materials Science and Engineering: C, 72 (2017), pp. 641–649.

[13] G. DRYHURST, *Electrochemistry of biological molecules*, Elsevier, 2012.

[14] D. FRAY AND C. SCHWANDT, *Aspects of the application of electrochemistry to the extraction of titanium and its applications*, Materials transactions, 58 (2017), pp. 306–312.

[15] V. FREGER AND S. BASON, *Characterization of ion transport in thin films using electrochemical impedance spectroscopy: I. principles and theory*, Journal of Membrane Science, 302 (2007), pp. 1–9.

[16] C. GABAY, *Interleukin-6 and chronic inflammation*, Arthritis research & therapy, 8 (2006), pp. 1–6.

[17] S. GLASSTONE, *An introduction to electrochemistry*, Read Books Ltd, 2011.

[18] D. C. GRAHAME, *The electrical double layer and the theory of electrocapillarity.*, Chemical reviews, 41 (1947), pp. 441–501.

[19] J. L. HAMMOND, N. FORMISANO, P. ESTRELA, S. CARRARA, AND J. TKAC, *Electrochemical biosensors and nanobiosensors*, Essays in biochemistry, 60 (2016), pp. 69–80.

[20] O. HORNYKIEWICZ, *Dopamine (3-hydroxytyramine) and brain function*, Pharmacological reviews, 18 (1966), pp. 925–964.

[21] S. HOU ET AL., *Highly sensitive and selective dopamine biosensor fabricated with silanized graphene*, The Journal of Physical Chemistry C, 114 (2010), pp. 14915–14921.

[22] Z. S. IRO, C. SUBRAMANI, S. DASH, ET AL., *A brief review on electrode materials for supercapacitor*, Int. J. Electrochem. Sci, 11 (2016), pp. 10628–10643.

[23] F. JAOUEN, G. LINDBERGH, AND G. SUNDHOLM, *Investigation of mass-transport limitations in the solid polymer fuel cell cathode: I. mathematical model*, Journal of the Electrochemical Society, 149 (2002), p. A437.

[24] L. JOTHI ET AL., *Simultaneous determination of ascorbic acid, dopamine and uric acid by a novel electrochemical sensor based on n2/ar rf plasma assisted graphene nanosheets/graphene nanoribbons*, Biosensors and Bioelectronics, 105 (2018), pp. 236–242.

[25] R. B. KEITHLEY, P. TAKMAKOV, E. S. BUCHER, A. M. BELLE, C. A. OWESSON-WHITE, J. PARK, AND R. M. WIGHTMAN, *Higher sensitivity dopamine measurements with faster-scan cyclic voltammetry*, Analytical chemistry, 83 (2011), pp. 3563–3571.

[26] P. T. KISSINGER AND W. R. HEINEMAN, *Cyclic voltammetry*, Journal of chemical education, 60 (1983), p. 702.

[27] C. M. KLINGE, *Estrogen receptor interaction with estrogen response elements*, Nucleic acids research, 29 (2001), pp. 2905–2919.

[28] A. KNOWLTON AND A. LEE, *Estrogen and the cardiovascular system*, Pharmacology & therapeutics, 135 (2012), pp. 54–70.

[29] S. KONOPKA AND B. MCDUFFIE, *Diffusion coefficients of ferri-and ferrocyanide ions in aqueous media, using twin-electrode thin-layer electrochemistry*, Analytical Chemistry, 42 (1970), pp. 1741–1746.

[30] L. S. KUMAR ET AL., *Label free nano-aptasensor for interleukin-6 in protein-dilute bio fluids such as sweat*, Analytical Methods, 8 (2016), pp. 3440–3444.

[31] T. J. LANG, *Estrogen as an immunomodulator*, Clinical immunology, 113 (2004), pp. 224–230.

[32] A. LASIA, *Electrochemical impedance spectroscopy and its applications*, Springer, 2002.

[33] J. A. LEE, S. HWANG, J. KWAK, S. I. PARK, S. S. LEE, AND K.-C. LEE, *An electrochemical impedance biosensor with aptamer-modified pyrolyzed carbon electrode for label-free protein detection*, Sensors and Actuators B: Chemical, 129 (2008), pp. 372–379.

[34] X. LI, Z. HUANG, C. E. SHUCK, G. LIANG, Y. GOGOTSI, AND C. ZHI, *Mxene chemistry, electrochemistry and energy storage applications*, Nature Reviews Chemistry, 6 (2022), pp. 389–404.

[35] Y. LIU ET AL., *Superb electrically conductive graphene fibers via doping strategy*, Advanced Materials, 28 (2016), pp. 7941–7947.

[36] W. LUO, F. SHEN, C. BOMMIER, H. ZHU, X. JI, AND L. HU, *Na-ion battery anodes: materials and electrochemistry*, Accounts of chemical research, 49 (2016), pp. 231–240.

[37] R. MAEXA, *Nernst-planck equation*, Encyclopedia of computational neuroscience, (2022), pp. 2182–2187.

[38] B. D. MCCLOSKEY, D. S. BETHUNE, R. M. SHELBY, G. GIRISHKUMAR, AND A. C. LUNTZ, *Solvents' critical role in nonaqueous lithium–oxygen battery electrochemistry*, The Journal of Physical Chemistry Letters, 2 (2011), pp. 1161–1166.

[39] P. NAYAK ET AL., *Highly efficient laser scribed graphene electrodes for on-chip electrochemical sensing applications*, Advanced Electronic Materials, 2 (2016), p. 1600185.

[40] R. S. NICHOLSON, *Theory and application of cyclic voltammetry for measurement of electrode reaction kinetics.*, Analytical chemistry, 37 (1965), pp. 1351–1355.

[41] S. NILSSON, S. MAKELA, E. TREUTER, M. TUJAGUE, J. THOMSEN, G. ANDERSSON, E. ENMARK, K. PETTERSSON, M. WARNER, AND J.-Å. GUSTAFSSON, *Mechanisms of estrogen action*, Physiological reviews, 81 (2001), pp. 1535–1565.

[42] J. K. NOVEV AND R. G. COMPTON, *Natural convection effects in electrochemical systems*, Current Opinion in Electrochemistry, 7 (2018), pp. 118–129.

[43] M. E. ORAZEM AND B. TRIBOLLET, *Electrochemical impedance spectroscopy*, New Jersey, 1 (2008), pp. 383–389.

[44] S. PALANISAMY ET AL., *Facile synthesis of cellulose microfibers supported palladium nanospindles on graphene oxide for selective detection of dopamine in pharmaceutical and biological samples*, Materials Science and Engineering: C, 98 (2019), pp. 256–265.

[45] N. PEREZ AND N. PEREZ, *Mass transport by diffusion and migration*, Electrochemistry and Corrosion Science, (2016), pp. 151–197.

[46] K. PETTERSSON AND J.-Å. GUSTAFSSON, *Role of estrogen receptor beta in estrogen action*, Annual review of physiology, 63 (2001), pp. 165–192.

[47] M. POURBAIX, *Applications of electrochemistry in corrosion science and in practice*, Corrosion Science, 14 (1974), pp. 25–82.

[48] S. PRUNEANU ET AL., *The influence of uric and ascorbic acid on the electrochemical detection of dopamine using graphene-modified electrodes*, Electrochimica Acta, 154 (2015), pp. 197–204.

[49] S. RANI, W. ABDULLAH, Z. ZAIN, AND N. AQMAR, *Integrated circuit design of 3 electrode sensing system using two-stage operational amplifier*, in IOP Conference Series: Materials Science and Engineering, vol. 340, IOP Publishing, 2018, p. 012017.

[50] P. H. RIEGER, *Electrochemistry*, Springer Science & Business Media, 1993.

[51] M. ROTHAUG, C. BECKER-PAULY, AND S. ROSE-JOHN, *The role of interleukin-6 signaling in nervous tissue*, Biochimica et Biophysica Acta (BBA)-Molecular Cell Research, 1863 (2016), pp. 1218–1227.

[52] M. SAJID, N. BAIG, AND K. ALHOOSHANI, *Chemically modified electrodes for electrochemical detection of dopamine: Challenges and opportunities*, TrAC Trends in Analytical Chemistry, 118 (2019), pp. 368–385.

[53] A. SMITH, J. BURNS, D. XIONG, AND J. DAHN, *Interpreting high precision coulometry results on li-ion cells*, Journal of The Electrochemical Society, 158 (2011), p. A1136.

[54] D. J. TYRRELL AND D. R. GOLDSTEIN, *Ageing and atherosclerosis: vascular intrinsic and extrinsic factors and potential role of il-6*, Nature Reviews Cardiology, 18 (2021), pp. 58–68.

[55] J. J. VAN BENSCHOTEN, J. Y. LEWIS, W. R. HEINEMAN, D. A. ROSTON, AND P. T. KISSINGER, *Cyclic voltammetry experiment*, Journal of Chemical Education, 60 (1983), p. 772.

[56] J. VAN SNICK, *Interleukin-6: an overview*, Annual review of immunology, 8 (1990), pp. 253–278.

[57] S. WALL, *The history of electrokinetic phenomena*, Current Opinion in Colloid & Interface Science, 15 (2010), pp. 119–124.

[58] S. WANG, J. ZHANG, O. GHARBI, V. VIVIER, M. GAO, AND M. E. ORAZEM, *Electrochemical impedance spectroscopy*, Nature Reviews Methods Primers, 1 (2021), p. 41.

[59] W. WANG ET AL., *Enhanced catalytic and dopamine sensing properties of electrochemically reduced conducting polymer nanocomposite doped with pure graphene oxide*, Biosensors and Bioelectronics, 58 (2014), pp. 153–156.

[60] K. R. WATERS, J. MOBLEY, AND J. G. MILLER, *Causality-imposed (kramers-kronig) relationships between attenuation and dispersion*, IEEE transactions on ultrasonics, ferroelectrics, and frequency control, 52 (2005), pp. 822–823.

[61] S. WHITE AND U. TWARDOCH, *The chemistry and electrochemistry associated with the electroplating of group via transition metals*, Journal of applied Electrochemistry, 17 (1987), pp. 225–242.

[62] R. A. WISE, *Dopamine, learning and motivation*, Nature reviews neuroscience, 5 (2004), pp. 483–494.

[63] Y.-X. YIN, S. XIN, Y.-G. GUO, AND L.-J. WAN, *Lithium–sulfur batteries: electrochemistry, materials, and prospects*, Angewandte Chemie International Edition, 52 (2013), pp. 13186–13200.

[64] K. ZHANG, G. LIU, AND E. M. GOLDYS, *Robust immunosensing system based on biotin-streptavidin coupling for spatially localized femtogram ml^{-1} level detection of interleukin-6*, Biosensors and Bioelectronics, 102 (2018), pp. 80–86.

[65] S. ZHANG, G. WRIGHT, AND Y. YANG, *Materials and techniques for electrochemical biosensor design and construction*, Biosensors and Bioelectronics, 15 (2000), pp. 273–282.

[66] W. ZHANG, D. WANG, AND W. ZHENG, *A semiconductor-electrochemistry model for design of high-rate li ion battery*, Journal of Energy Chemistry, 41 (2020), pp. 100–106.

[67] C. G. ZOSKI, *Handbook of electrochemistry*, Elsevier, 2006.

BIOGRAPHICAL SKETCH

In May 2023, Dipannita Ghosh accomplished the Master of Science in Electrical Engineering program at the University of Texas Rio Grande Valley (UTRGV). She was bestowed with the prestigious Presidential Graduate Research Assistantship in 2021. During her academic tenure, she worked under the supervision of Dr. Nazmul Islam & Dr. Ali Ashraf and contributed as a research assistant in the Electrical Engineering Department.

Dipannita will continue her academic journey by pursuing a PhD in Materials Science at UT Dallas in Fall 2023. His primary research interests include semiconductor device characterization. Should you require additional information or assistance, Dipannita can be contacted through email at dipannita.buet.14@gmail.com.